ACOUSTIC EMISSION STUDIES OF SLOW CRACK GROWTH IN Zr-2.5% Nb

by

ARVIND ARORA

A Thesis

Submitted to

The Faculty of Graduate Studies

In Partial Fulfillment

of the Requirements for the Degree of

Master of Science

in

Mechanical Engineering

Department of Mechanical Engineering

University of Manitoba

Winnipeg, Manitoba

September, 1978

ACOUSTIC EMISSION STUDIES OF SLOW CRACK GROWTH IN Zr-2.5% Nb

BY

ARVIND ARORA

A dissertation submitted to the Faculty of Graduate Studies of the University of Manitoba in partial fulfillment of the requirements of the degree of

MASTER OF SCIENCE

INDEX

ABSTRACT

The detection and analysis of 'Acoustic Emission' is one of the most promising non-destructive techniques to be used as an integrity monitoring device. The technique has the ability to detect the crack formation and its growth, at the time it occurs, and to accomplish this remotely.

Acoustic emission could be classified as low amplitude acoustic signals emanating from processes involving small amounts of energy such as plastic deformation, twinning, slip or sudden reorientation of grain boundaries and as high amplitude signals from micro/macro cracking, fatique, stress corrosion cracking, and hydrogen embrittlement, etc. Dealing with high amplitude signals, as they are easy to handle with respect to the noise level of the system, the AE has a vital potential to monitor sub-critical crack growth.

The mechanism in Zr, Ti and Va alloys involves discontinuous crack extension through hydride particles formed at certain temperatures in the presence of available hydrogen and is usually termed as delayed hydride cracking. AE was successfully monitored for slow crack growth during delayed hydride cracking in Zr-2.5% Nb alloy. The results indicate that the quantitative measurements of crack extension and crack velocity, which is of the order 10^{-9} to 10^{-11} m/sec, are possible using acoustic emission technique. Furthermore, AE tests support the suggested fracture mechanism in this alloy.

The effects of stress intensity, temperature and hydrogen content have been studied on acoustic response of slow crack growth and discussed accordingly. The total number of counts and the burst count rate were found to be in direct proportionality with the area cracked during slow crack growth and the crack velocity respectively.

ACKNOWLEDGEMENT

The author wishes to express sincere thanks to Dr. K. Tangri for his supervision. Special thanks are due to Dr. L.A. Simpson for valuable discussions and to AECL for supplying the material and specimens. Messrs. D. Mardis and J.R. Sill are acknowledged for their help.

LIST OF FIGURES

Page

LIST OF PLATES

LIST OF TABLES

1. INTRODUCTION

Slow crack growth has been observed in various materials such as steels, nickel, Ti, Va, Zr, etc. under hydrogen embrittlement. Stress corrosion cracking and fatigue. Various techniques have been employed to measure crack velocity during slow crack growth in these materials. One of the most common techniques for such measurements involves the use of COD (crack opening displacement) gauge. The technique provides reasonably reliable data as far as crack velocity measurements are concerned. However, COD measurements reflect only the cumulative effect of all crack growth events in the thickness, i.e. the macroscopic crack growth. (The use of COD gauge also involves specimen standardization and calibrations). Optical method has been used to monitor the moving crack tip by employing a travelling microscope. This method reveals only the surface effects and cannot be used in the case of plain strain fracture toughness tests where the crack growth is more dominant at the centre of the specimen. This method may also produce erroneous results where the crack branching is associated with the crack tip movement. Other researchers[1,3] have used a post-mortem type of technique where the specimen is fast fractured after the test and the incremental crack growth optically measured. This technique is very time consuming and measures only the cumulative growth for a certain length of time. The above techniques suffer from a common handicap, namely, their

limited potential in determining the details of the fracture mechanisms involved.

In this study, acoustic emission has been advantageously used for the detection and continuous surveillance of propagating cracks in Zr-2.5% Nb. An AE testing system has been developed to test fatigue precracked compact tension specimens and AE signals from slow crack growth have been analyzed. The AE count rate provided quantitative measurements of crack growth rates while totalized AE (burst*) counts estimated the incremental area cracked. The nature of AE plots from the slow crack growth indicated that the crack growth process was discontinuous and involved local embrittlement. The absence of AE bursts at temperatures above 200°C in isothermal SCG test indicate the requirement of hydride particle for crack growth to occur. These observations confirmed the basic models of slow crack growth in this material, suggested by AECL researchers[42-46]. Effects of stress intensity factor, temperature and hydrogen content were studied and have been discussed accordingly. Supplementary fractographic studies employing optical, scanning and transmission electron microscopes were carried out on AE tested specimens. These studies further confirmed the conclusions that the crack growth process is intermittent and involves hydride cracking.

---

* See Appendix C

2. LITRATURE SURVEY

2.1 Acoustic Emission

Acoustic emission is a natural concomitant of any dynamical process. The stored potential energy during straining of the material is released during deformation and fracture. Part of this energy is transformed into elastic waves that propagate through the material and may be detected on the surface by a sensitive transducer. Such signals are called acoustic signals, stress wave emissions or seismic signals. These emissions are high frequency (10 KHz to 5MHz), short time (.03 to 30 μsec) pulses which reflect the response of the material under deformation.

Characteristically, all metals exhibit two distinct types of emissions[23,25,30] referred to as burst type and continuous type (Fig. 1). As observed on the oscilloscope screen, the burst type signal appears as an exponentially decaying ring down pulse, with relatively high amplitude whereas the continuous signal has an appearance of sustained signal level with relatively low amplitude. The two emissions are produced depending on (1) AE response of the material, e.g. zinc emanates predominantly burst type while Aluminum almost entirely continuous signals; (2) type of deformation, e.g. micro/macro cracking and fracture result in burst type while yielding and plastic deformation produce continuous emissions. A large number of investigations have been reported on AE generation during

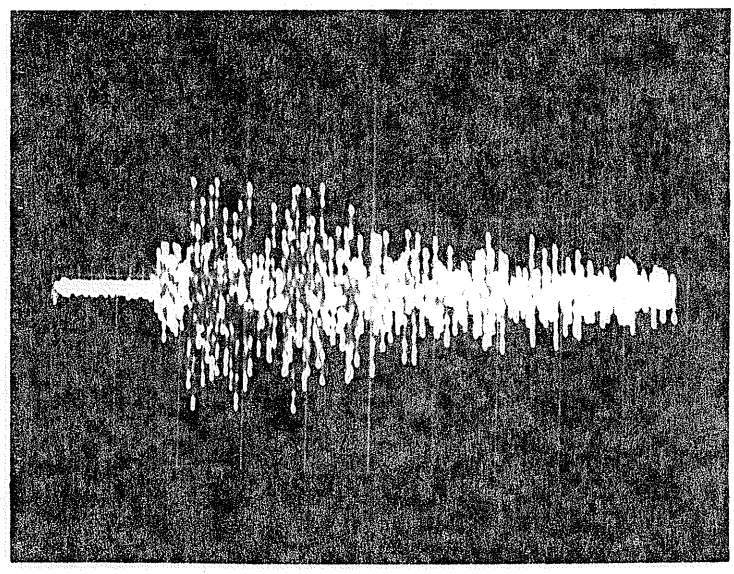

(a) Burst type signals

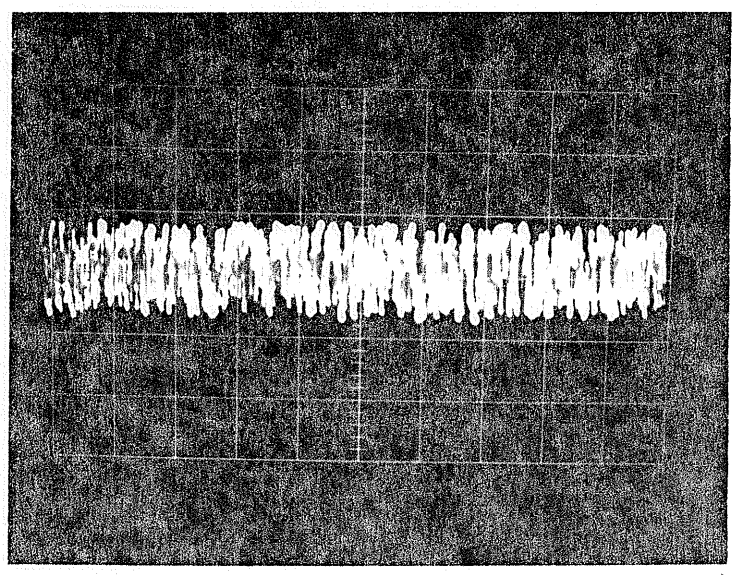

(b) Continuous signal

FIGURE 1. Characteristic Emissions from Metals

plastic deformation, initiation and propagation of flaws in a variety of materials[5-20]. A historical review of research in AE has been presented by Liptai et al[4].

Recent applications of the technique have been mainly in two fields, 1) basic materials research and 2) applied structural integrity.

2.1.1 AE and Basic Materials Research

As this area is not of direct concern in this investigation, only a brief review is presented for the sake of completion and to provide the more significant references to literature. Attempts have been made to identify the sources of AE during deformation of single crystals, polycrystalline materials and composite materials. Fisher and Lally[5] and many other researchers[6,7,8] have identified dislocation motion as a prime source of acoustic emission. Gillis[9] has presented a model to support dislocation motion as a source of acoustic emission. Speich and Fisher[10] have observed that martensitic transformation produces acoustic emission. Liptai et al[11] also related acoustic emission to martensitic transformation in Au-Cd, In-Ti and in cobalt during fast cooling. Woodward and Harris[12] used signal analysis to identify sources of acoustic emission. In the recent studies by Gillis and Hamstad[13] a relationship has been developed between acoustic emission and the amount of deformation. Tandon and Tangri[14] used acoustic emission technique to study dislocation generation from grain boundaries. Various processes giving rise to acoustic emission may be tabulated in

the following form[15]:

MICROSCOPIC PROCESSES	MACROSCOPIC PROCESSES
Creep	Boiling detection and bubble formation
Dislocation Movement	Etching
Embrittlement	Crack growth
Luderband formation	Fracture
Magnetic transition	Leak detection
Ferroelectric transition	Welding
Slipping	Corrosion
Twinning	Thermal shocks

2.1.2 AE and Structural Integrity

Considerable amount of work has been done to use AE as a means of evaluating structural integrity by detecting active flaws which may cause ultimate failure. Evans and Linzer[16] used AE for failure prediction in structural ceramics. A substantial amount of emissions was obtained well before fracture and increasing acoustic emission count rate predicted the incipient failure. Structural integrity of fiber/epoxy vessels was investigated by Hamstad and Chiao[17] by developing an AE monitoring system to detect flaws leading to the structural failure. Webborn and Rawlings[18] detected fatique cracking prior to catastrophic failure by AE monitoring of welded tubular joints under constant and random amplitude loads. Hartbower et al[19] used AE as a precursor of imminent failure for low

cycle fatique and environmentally assisted fatique in a similar manner, by detecting cracking and crack growth.

During tensile testing of flawed and unflawed specimens of 7075-T6 Al, Dunegan and Harris[20] found that the AE count is a function of plastic volume in flawed specimens. Alternatively, Palmer and Heald[21] suggested that the total emission count is a function of the area of elastic plastic boundary ahead of the crack and not the plastic volume. They postulated that total emission count, N, is directly proportional to the plastic zone radius, S, such that

$$N = D \cdot S \tag{2.1}$$

where D is the proportionality constant depending on strain rate, temperature, thickness and microstructure. In linear elastic fracture mechanics, the plastic zone is proportional to the square of stress intensity factor, K,

$$N \propto K^2 \tag{2.2}$$

A more generalized relation was suggested by Dunegan et al[22] in the form:

$$N \propto K^m \tag{2.3}$$

where exponent m was found to vary between 2 to 8, typically 4 for 7075-T6 Al, and 8 for Berillium. Their tests on signle edge notch fracture toughness specimens followed this exponential relation.

Gerberich and Hartbower[23] have found a relationship between crack parameters and acoustic emission. A semi-empirical relationship was developed from elasticity theory

$$\Delta A \sim (\Sigma g)^2 \, E/K^2 \tag{2.4}$$

where ΔA is the incremental area swept out by the crack, Σg is the sum of stress wave amplitudes, E is the elastic modulus, and K is the applied stress intensity factor. They compared the results from fatique tests on steels, Al and Ti, (Fig.2) and found that a reasonable correlation exists between Σg/cycle and crack growth increment/cycle. The above formulation was semi-quantitative in nature and assumed an infinite plate geometry for a relatively narrow specimen. Gerberich et al[24] also proposed

$$g \simeq \frac{2\Delta AK^2}{C_1 EL} \qquad (2.5)$$

where C_1 is a constant, and L is the sample length between grips.

Dunegan and Tetelman[25] conducted experiments on cathodically charged steels to monitor hydrogen embrittlement. They found acoustic emission (AE) and crack opening displacement (COD) to be linear functions of time. They also developed a relationship between AE count rate and stress intensity factor:

$$\frac{dN}{dt} = 6.66 \times 10^{-5}(K^5 - K_o^5) \qquad (2.6)$$

where K_o is the threshold stress intensity factor ($7 KSi/in^{1/2}$). The most important conclusions reached in this study was that the AE rate can be used to determine the time for the onset of rapid fracture and corresponding stress intensity factor, regardless of initial loading, incubation time or any other factors connected with geometrical differences. Using a

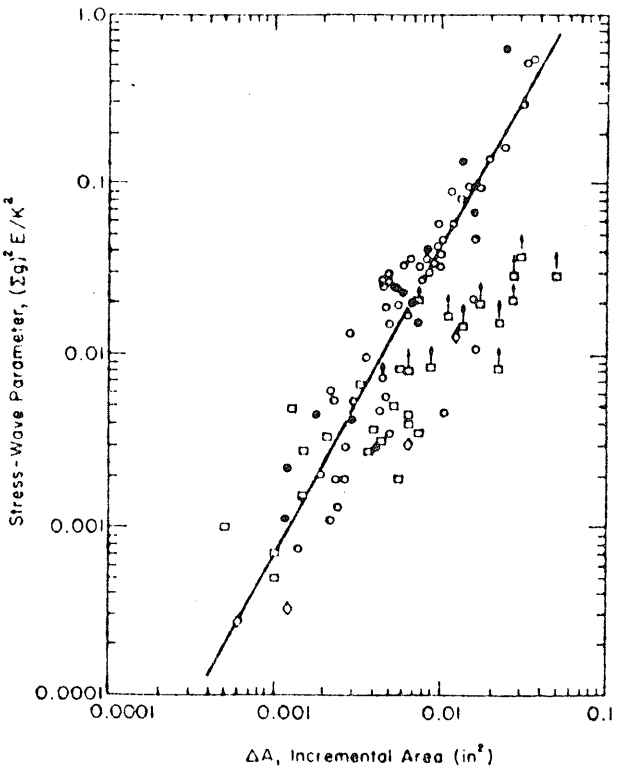

FIGURE 2. Stress Wave Parameter Versus Incremental Crack Area for Certain Materials. O,D6aC Steel-High Stress Intensity Fatique; ●,D6aC Steel-Environmental Cracking Under Sustained Loads; □ ,7075T6 Aluminum-Rising Load; ◇ , 5AL-4V Titanium-Rising Load[23].

slightly different technique Harris et al[26] reported slow crack growth in steels under hydrogen embrittlement or fatique conditions to follow a relationship

$$\frac{dN}{dA} = D \cdot K^n \qquad (2.7)$$

where $\frac{dN}{dA}$ is AE count per unit area fractured, D and n are constants.

Since the stress intensity factor is related to plastic zone size and the latter is further related to crack tip opening displacement, acoustic emission could be characterized in terms of crack opening displacement. This was attempted by Palmer et al[27] for compact tension steel specimen. They showed that the total AE counts and COD bear a relationship of the form

$$N = A\delta^h \qquad (2.8)$$

where δ is the crack opening displacement and A is a constant. The exponent n was found to be close to unity in their experiments. Similar results have been reported by Bentley et al[28,29]. They observed values of approximately 1.2 for a similar C/Mn pressure vessel and for a Mo/B steel.

Evans and Linzer[30,31], in their study on porcelain and alumina, showed that AE count rate, $\dot{N}$, is directly proportional to the crack velocity, V:

$$\dot{N} \propto V \qquad (2.9)$$

Theoretically, the crack velocity is proportional to the stress intensity, so

$$V = \alpha K_I^n \tag{2.10}$$

where α and n are constants. From equations (2.9) and (2.10) the AE count rate is related to crack tip stress intensity in the following form:

$$\dot{N} = \beta K_I^h \tag{2.11}$$

where β is another constant. The experimental results indicate that for porcelain and alumina, $n \simeq m$ of equation (2.3). Nadeau[32] observed similar relationship between AE count rate and crack velocity for pocco graphite. He also stated that for a given material, the number of counts per unit area should be constant no matter how rapid the crack grows.

Other studies in the area of slow crack growth that have been reported are: (i) in D6Ac steel under hydrogen embrittlement and fatique conditions (by Gerberich and Hartbower[33]), (ii) in titanium alloys under stress corrosion cracking (by Cox[34] and Katz and Berberich[35]), and (iii) in 304 stainless steel under stress corrosion cracking (by Brihmadesam and McCormic[36]). The important features of these studies are summarized below:

(1) The crack growth could be monitored by AE, as it occurs. Fig. 3[37] shows a schematic of the crack jump in AE monitoring; primary incubation period and successive crack jumps are evident.

(2) The effect of corrosive conditions and test parameters (temperature, stress and heat treatment) could be studied by AE tests.

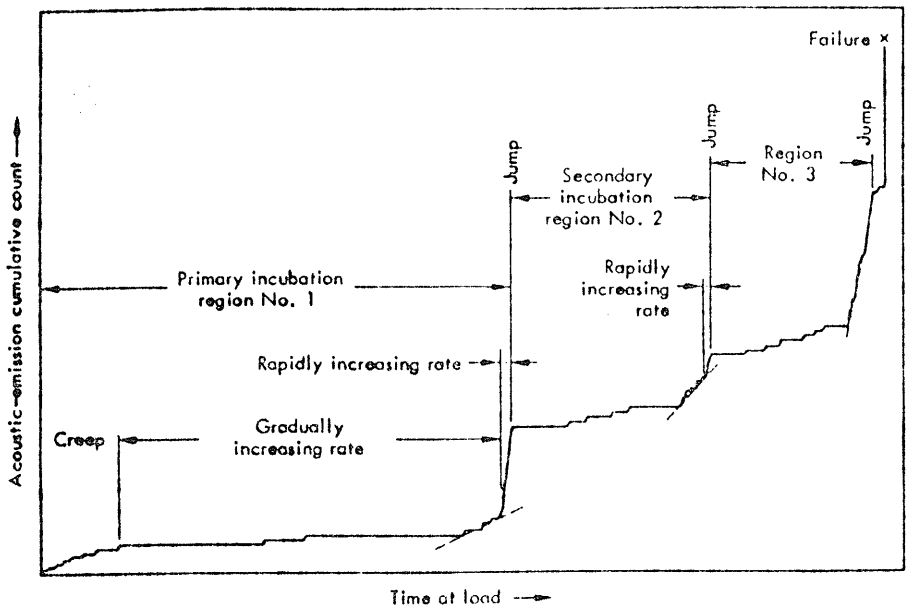

FIGURE 3. Cumulative Acoustic Emission Count Versus Time at Constant Load during Stress Corrosion Cracking[37]

(3) Fracture mechanism could be identified and failure rates determined by AE studies to predict catastrophic failures.

Acoustic emission technique also has promise in the area of quality assurance testing and in process fabrication testing. Drouillard et al[38] have extended its application to the industrial use of AE for NDT quality assurance programs.

2.2 Fracture Behaviour of Zr-2.5% Nb

The delayed failure of cold worked Zr-2.5% Nb has been studied quite extensively by AECL researchers[39-43]. The fracture mechanism has been identified and quantitative measurements of the crack velocity have been made. Quantitative models to explain the sub-critical crack growth in Zr-2.5% Nb have been developed. Pertinent results of the above investigations are reviewed in the following three sections.

2.2.1 Fracture Mechanism

The hydrogen induced delayed failure has been reported in Zr-2.5% Nb[39-46]. In view of the experimental observations (discussed later), models[40-42,46] have been developed for short range diffusion of hydrogen and its precipitation in the form of hydrides under elevated stresses at the crack tip. It is postulated that in hydride forming materials such as Zr, Ti and Va, etc., hydrogen diffuses from sources (removed from the crack tip) to the vicinity of the stressed crack tip and hydride precipitates are formed. The crack then advances through the brittle hydride phase and is temporarily arrested.

The process then repeats itself. Thus resulting in intermittent growth of a crack. Direct, in situ, observations using HVEM have been reported which confirm this process in the case of Va[47].

The models[42,46] developed for hydrogen assisted crack growth assume that, in steady state condition, the crack growth rate is equal to the derived rate of growth of the hydride precipitate. It is a reasonable assumption because the kinetics of crack propagation is controlled by the growth of hydrides at the crack tip by the diffusion of hydrogen into this region. Simpson and Ells[48] have calculated diffusion controlled growth rates of hydride precipitates in the vicinity of the crack tip in Zr-2.5% Nb specimens. Further developments involving principles of fracture mechanics and effects of diffusional flux changes have been made Dutton and his co-workers[42,49], to describe the behaviour of crack advancement at various crack tip stress intensities. Their model calculates the rate of hydride growth and assumes that the latter controls the rate of crack propagation, thus measuring the crack velocity. This model did not explain the experimentally observed intermittent nature of the crack growth process but measured the rate of particle growth representing an average rate of crack velocity.

The hydrogen flux during diffusion was calculated considering hydrogen diffusion under various forces such as (1) thermo-

dynamic driving force*, (2) stress gradient around crack tip due to loading. The diffusion equation is

$$J_H = \frac{D_H}{\Omega_{Zr}}\{\nabla C_H + \frac{C_H}{RT}\nabla\phi\} \qquad (2.12)$$

where $\phi = V_H\{\frac{1}{3}\sum_{i=1}^{3}\sigma_{ii} + \frac{1}{2}\sum_{i=1}^{3}\frac{\sigma_{ii}^2}{E}$

and ϕ = energy term, (drift term) represents interaction energy of the migrating hydrogen with local stress field.

C_H = atom fractions of hydrogen in α-Zr,

D_H = diffusion coefficient of hydrogen in α-Zr,

Ω_{Zr} = atomic volume of Zr in α-Zr,

V_H = molal volume of hydrogen in α-Zr,

σ_{ii} = principal stress component near the crack tip (-ve if tensile),

E = elasticity modulus.

The final velocity expression derived from fracture mechanics using above diffusional equation led to --

$$v = \frac{\Pi\Omega \text{ hydride} \cdot D_H \cdot C_H^S}{1.6\ \ell'\ \phi\ \Omega_{Zr}} \exp\{P(L) \cdot \bar{V}_H^h/RT\} \times$$

$$\{1-\exp(\Delta p\ \bar{V}_H^h/RT)\} \qquad (2.13)$$

*Thermodynamic driving force results from energetically favoured precipitation of hydride because there is a large volume increase (~17%) when the zorcomium matrix is converted into the hydride phase.

where

Ω hydride = atomic volume of hydride in α-Zr,

$\bar{V}_H^h$ = molal volume of hydrogen in Zr hydride,

ℓ' = effective crack tip radius

$P(L)$ = the local hydrostatic stress at distance L,

$$= \frac{1}{3} \sum_{i=1}^{3} \sigma_{ii}(L)$$

$\Delta p = p(\ell) - p(L)$

C_H^s = terminal solubility of hydrogen in solution.

Assumptions were made that the crack is infinitely sharp and the material is perfectly brittle. A good correlation between experimental data and the derived velocity was observed. The development of the above model is still underway.

2.2.2 Sub-Critical Crack Growth

Slow crack growth in compact tension specimens of Zr-2.5% Nb has been observed at all temperatures between 25 to 325°C and at K_I values between 10 to 50 $MNm^{-3/2}$ during static loading[39-46]. The crack growth occurs under the influence of triaxial stress state at the crack tip. Experiments[39,40,45] conducted below 250°C, reveal a two stage behaviour of HIDC. As shown in Fig. 4[43], the crack velocity is strongly stress dependent in the first stage ($K_I \sim 5$-10 $MNm^{-3/2}$) and nearly

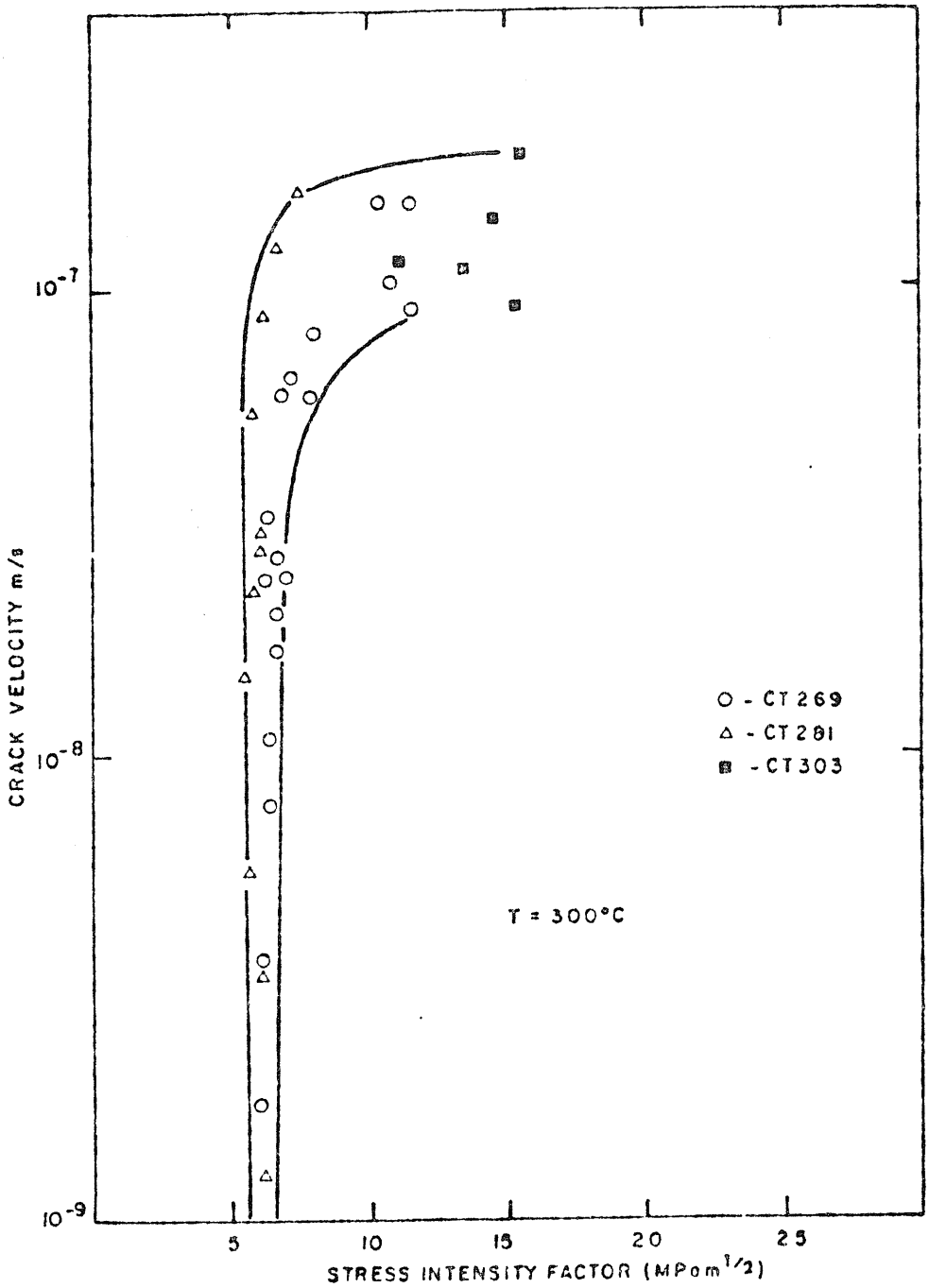

FIGURE 4. Crack Velocity Versus Stress Intensity Curve for Zr-2.5% Nb[43].

independent of stress in the second stage ($K_I > 10 MNm^{-3/2}$). In stage I, crack growth rate rises sharply with the increase in crack tip stress intensity where as it is more or less constant over the stress intensity range of stage II. A threshold stress intensity* has been ovserved in all experiments which is of the order 7-8 $MNm^{-3/2}$. In later developments[43,44] where the tests were preceded by a crack sharpening process, it has been observed that the threshold stress intensity is 6 $MNm^{-3/2}$ and for all loads above the threshold stress intensity the crack grows at more or less constant rate. The models developed for quantitative measurement of crack velocity have been discussed in the previous section.

The crack velocity increased with increase in temperature. However, no quantitative relationships could be developed due to large scatter in their data. At 250°C and above, the slow crack growth was not reproducible except after a thermal cycle. The thermal cycle produced a concentrated region of reoriented hydrides at the crack tip which significantly reduced the incubation period** for slow crack growth. Little or no crack growth observed above 250°C results from the dissolution of hydride particles at those temperatures. This observation indicates that the presence of hydrides is a primary requirement for crack growth to take place.

---

* Threshold Stress Intensity is the crack tip stress intensity below which no crack growth occurs for extended periods of loading.

** Incubation Period is the time to incubate cracking and crack growth after initial loading.

2.2.3 Fractography and Metallography

Fractography work has been conducted by Simpson and co-workers[41,45] to gain a better understanding of the fracture mechanism. The study of the fracture surface has been largely confined to stage II region of the V-K curve. Fractography has shown that the delayed hydrogen cracking in Zr-2.5% Nb occurs in an intermittent fashion. The main observations were of ductile striations and stretch zones parallel to the crack front with brittle, plate like regions between the striations. Some of these striation contained cleavage fracture between them. Each striation represented a period of crack arrest and crack blunting which was evident from the stretch zones associated with the striations. The interstriation spacing increased with increase in temperature indicating that the extent of hydride buildup at the crack tip is governed by local embrittlement required for crack advance. At higher temperatures, the Zr matrix is more ductile and as such requires a greater amount of hydrides for cleavage, which results in larger interstriation spacing. The general fracture morphology was essentially similar at all temperatures suggesting that a single fracture mechanism is operative over the range of temperatures studied. The stress dependence of the striation spacing has not been clearly established[39] but the results showed a weak dependence of stress intensity in stage II. This is consistent with the idea of low stress intensity dependence of crack velocity in stage II.

Enhanced crack growth was observed at the midsection of the specimen[39,41,45] in the slow crack growth region. This crack tunnelling was due to the triaxiality of stress state under plain strain condition.

Metallographic studies[39-42] revealed the accumulation of hydride precipitates near the crack tip. The hydride particles were normal to the applied stress. Thermal cycling showed significant effect on hydride reorientation. Accumulation of hydride particles was accelerated by a thermal cycle resulting in hydride clusters leading to further crack growth even above the temperatures of hydrogen solvus. Hydride coarsening has been also reported by Nuttal within the plastic zone during thermal cycling[39].

3. EXPERIMENTAL

3.1 Material and Specimen History

All the specimens were supplied by AECL and were made from pressure tube material (Zr-2.5% Nb). The tube was cut open and (cold) rolled flat and the compact tension (CT) specimens were cut to standard dimensions. The geometry and dimensions of the specimen are shown in Figure 5 with the type of loading. The specimen had a v notch and contained a sharp fatique crack at the root of the notch which served as a crack starter. The specimens were batched into two categories -- (i) unhydrided (ii) hydrided or treated samples. The unhydrided specimens contained nominal hydrogen, i.e. 5-10 ppm from the pressure tube and were annealed in vacuum at 400°C for 2 hours to relieve the residual stresses produced during cold rolling, machining and fatiguing. The specimens belonging to the second batch were hydrogenated in a closed chamber to increase its hydrogen content to 200 ppm, and were then homogenized for about 6 weeks at approximately 450°C. These specimens were not given annealing treatment for the reason that stress relieving took place during homogenization.

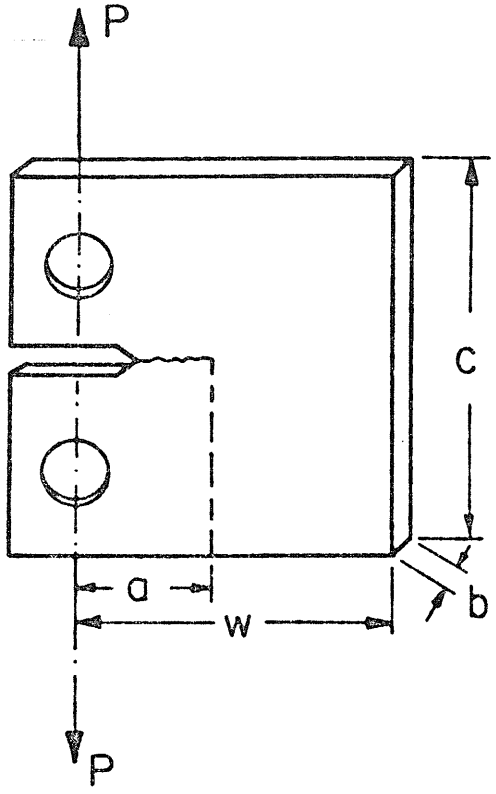

Dimensions
$w \simeq c \simeq 1.35$ in.
$a \simeq 0.60$ in.
$b \simeq 0.145$ in.

(a). Fatigue Precrack Test Specimen .

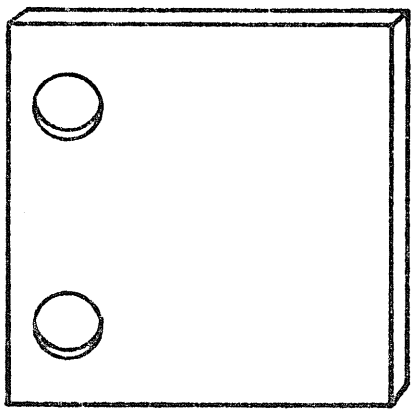

Dimensions :
Identical to Specimen
in Fig. a.

(b). A Dummy Specimen .

Fig.5. Geometry and Dimensions of CT Specimen

3.2 Crack Tip Stress Intensity Measurements

Specimens were polished to 1/4 micron finish and crack length measured under optical microscope. To obtain a given crack tip stress intensity, the required load was calculated from the following equation[50].

$$K_Q = (P_Q/bw^{\frac{1}{2}})\left[29.6\left(\frac{a}{w}\right)^{\frac{1}{2}} - 185.5\left(\frac{a}{w}\right)^{\frac{3}{2}} + 655.7\left(\frac{a}{w}\right)^{\frac{5}{2}} - 1017.0\left(\frac{a}{w}\right)^{\frac{7}{2}} + 638.9\left(\frac{a}{w}\right)^{\frac{9}{2}}\right] \quad (3.1)$$

where P_Q = load in lbs

b = thickness of specimen in inches

w = width of specimen in inches, and

a = crack length in inches.

To facilitate calculation of K_Q, values of power series given in the bracket in the above expression are tabulated in Table 1[50] for specific values of a/w.

Table 1

(a/w)	f(a/w)	(a/w)	f(a/w)	(a/w)	f(a/w)
0.450	8.34	0.485	9.19	0.520	10.21
0.455	8.45	0.490	9.33	0.525	10.37
0.460	8.57	0.495	9.46	0.530	10.54
0.465	8.69	0.500	9.60	0.535	10.71
0.470	8.81	0.505	9.75	0.540	10.89
0.475	8.93	0.510	9.90	0.545	11.07
0.480	9.06	0.515	10.05	0.550	11.26

3.3 Equipmental Set-Up

An acoustic-emission system capable of monitoring slow crack growth was designed and developed. The shematic of the experimental set-up is shown in Figure 6 and is discussed below.

3.3.1 Loading Mechanism

A lever beam mechanism was used for static (sustained) loading. The weights were applied onto the weight pan and the specimen was loaded in the jig as shown in Figure 6. The jig holding the specimen was enclosed in a small furnace to heat up the specimen when required. A DC power supply (Nobatron T 60-5) with output of 5 amps was employed for heating the furnace and had a precise control of $\pm$ 1°C in temperature. A chart recorder (Phillips type PR7791/001) was used to record the temperature continuously. An iron-constanton thermocouple was used to measure the specimen temperature. The specimen was isolated at all contacts with the loading jig by using a non-conducting tape on the pins.

3.3.2 Transducer

A peizoelectric (PZT) transducer (D 9205M2 Dunegan research corp.) was mounted on the specimen to detect AE signals. A refractory disc (Al_2O_3) was used to insulate the sensor from the specimen. High temperature vacuum grease was used on the mounting surface to avoid signal attenuation due to the presence of air film at contacts. The transducer had a maximum sensitivity at 93.9 db. Other transducer

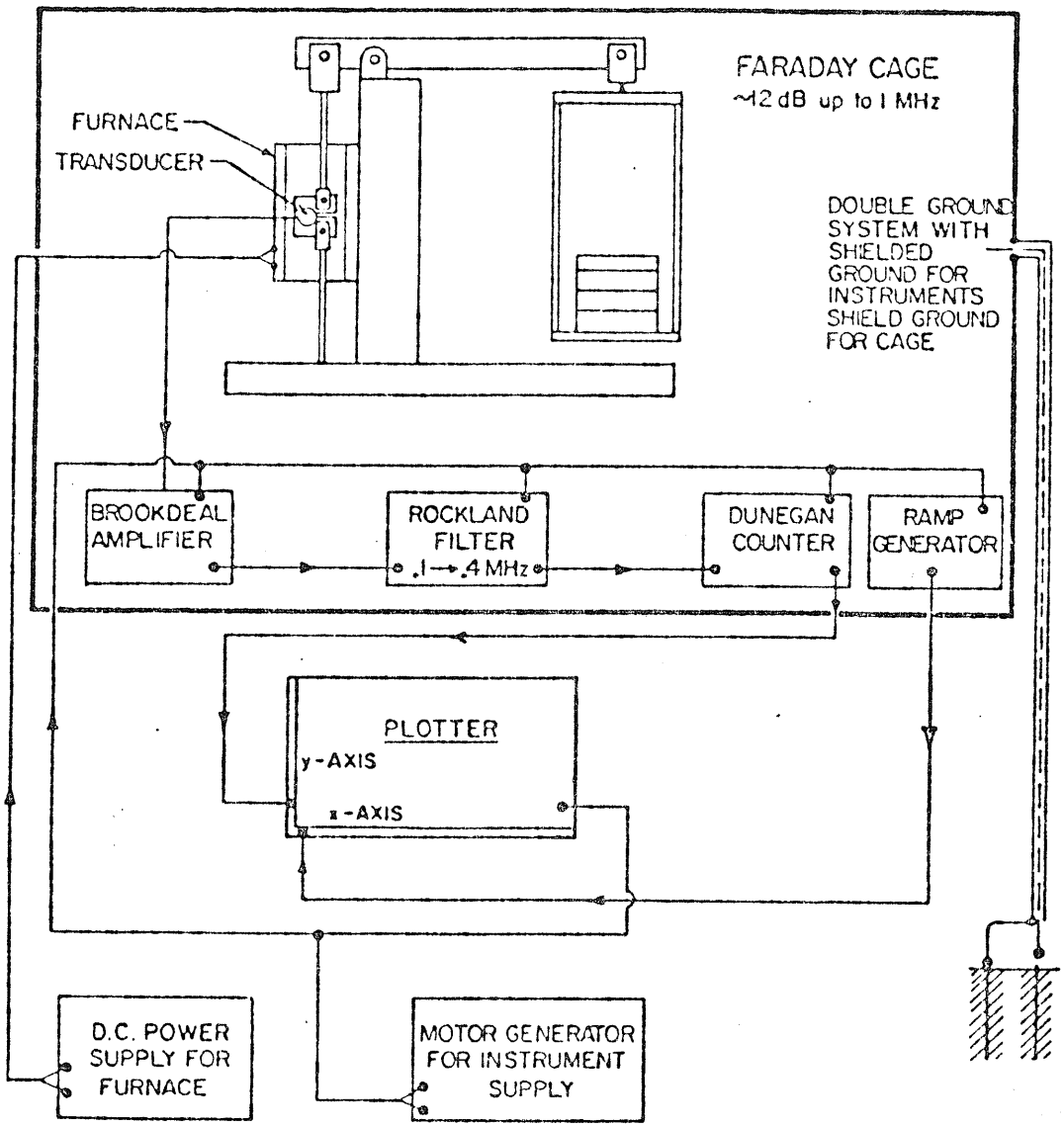

Fig. 6 BLOCK DIAGRAM OF THE AE TEST EQUIPMENT.

characteristics are given in Appendix A. The transducer had a low relative response above 400 KH_z. The characteristic response of the transducer was more or less same at temperatures up to 1000°F.

3.3.3 Premplifier and Filter

Differential AC amplifier (Brookdeal model 9454) was used as a preamplifier. It had a calibrated gain facility of 0 to 100 db and could be used with single ended or differential transducers. The preamplifier had a built-in filter with selectable frequencies. An electronic filter (Rockland model 1100) was used to filter out noise from the amplified signal. The filter had adjustable low and high band pass/ reject facility such that the signal could be bypassed over a range of frequencies or could be rejected for certain frequency range.

3.3.4 Signal Counter and Ramp Generator

This equipment was used for signal processing and plotting. The signal counter is designed to count the signal by ring down counting mechanism over an adjustable threshold voltage (1 volt in our case). The count totalizer (model NS-1, Dunegan research corp.) was provided with fixed and calibrated gain (maximum gain - 40 db). The ramp generator (model CR-11, Dunegan research corp.) had a facility of generating a continuous time ramp of 1 minute to 48 hours selectively.

3.3.5 Accessories

To continuously monitor the AE signal an x-y recorder was used. The power to all the equipment was supplied by a motor-generator assembly which had two output windows of 110 V supply up to 14 ampere loads. A biomation system was employed to trace the AE signals on the oscilloscope. The system (model 805 waveform recorder and 7613 oscilloscope) had adjustable time-voltage axes for the transient signals and a built in trigger system which facilitated in capturing signals of desired amplitude. All the equipments except biomation model and plotter were encaged in a faraday cage as shown in Figure 6. The cage had its own grounding system and protected the AE monitoring system from any external signals or noise. The cage shielded the system against radio and other high frequency signals. A six-volt DC signal generator was also used for system calibration purposes. Vickers (fifty-five) microscope, scanning electron microscope and Phillips 300 Transmission Electron microscope were used for fractography purposes.

3.4 Calibration and Test Procedure

The specimen was mounted in the jig, as shown in Plate 1 in fracture mode I. The transducer was fastened onto the specimen with a clamp unit. The experimental set-up was made according to the line diagram shown in Figure 6. As seen in Plate 2, the transducer was connected to the preamplifier (right top) and to the filter (right bottom) and then to the

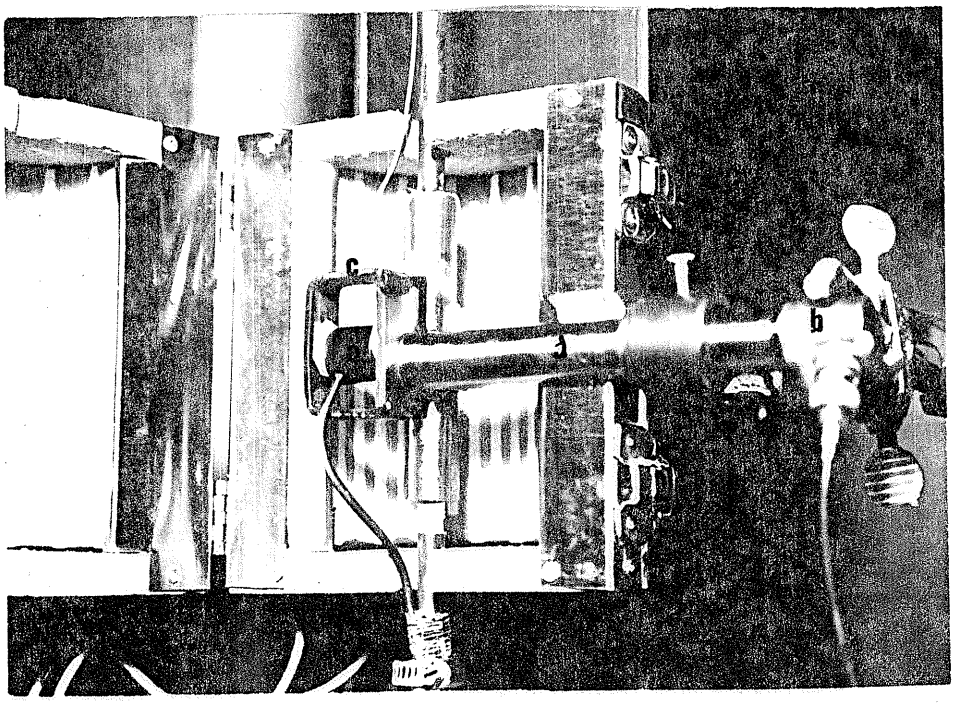

PLATE 1. CT Specimen in Jig With Mounted Transducers

a. test transducer, b. calibration transducer

c. transducer clamp, d. wave guide

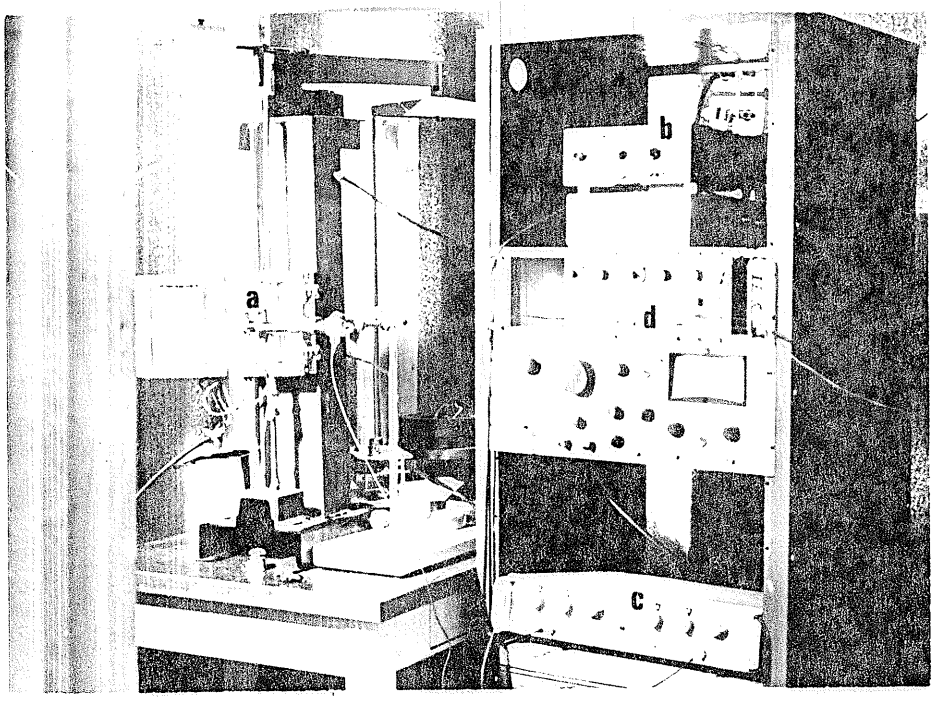

(i) Loaded specimen (a) with preamplifier (b), filter (c) and count totalizer (d).

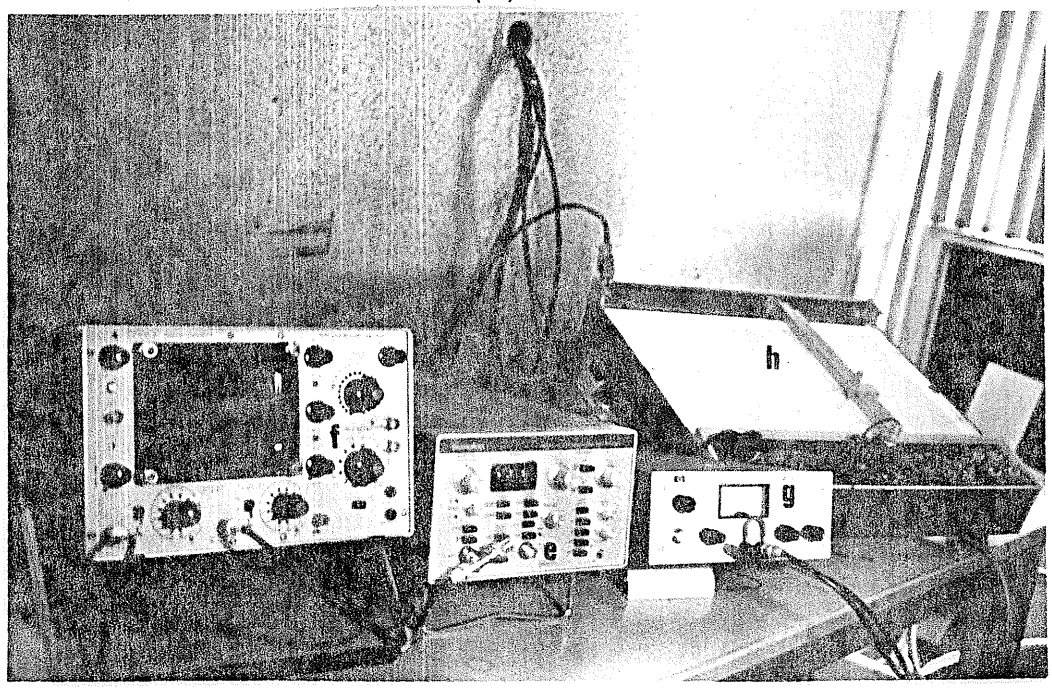

(ii) Biomation system (e) with oscilloscope (f), standard pulse generator (g) and chart recorder (h)

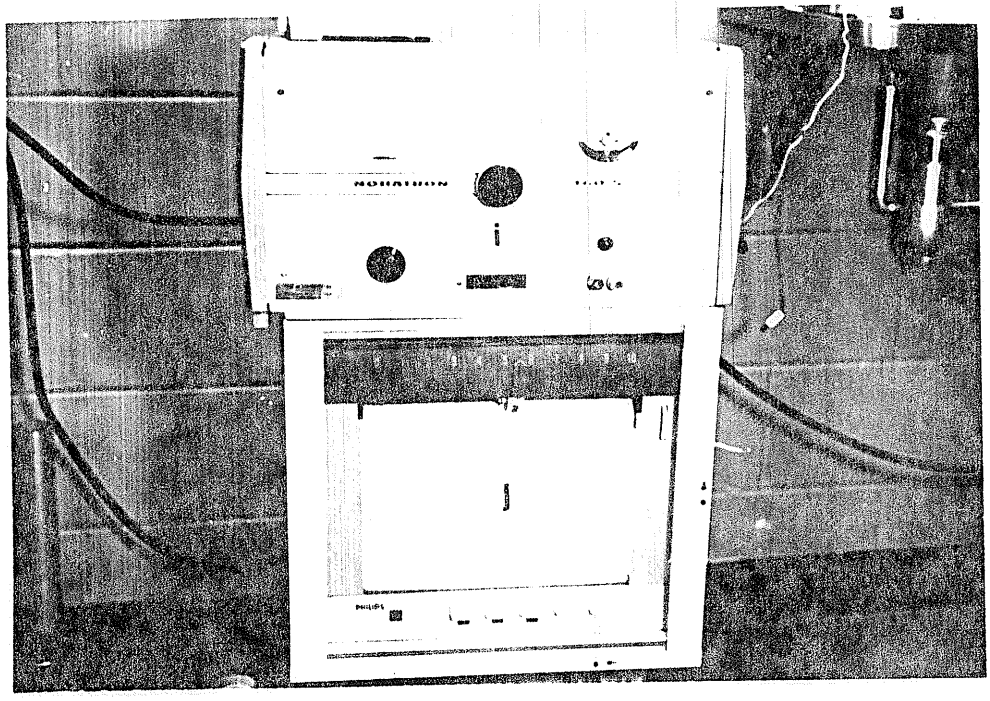

(iii) dc power supply for heating the furnace (i) and temperature monitor (j)

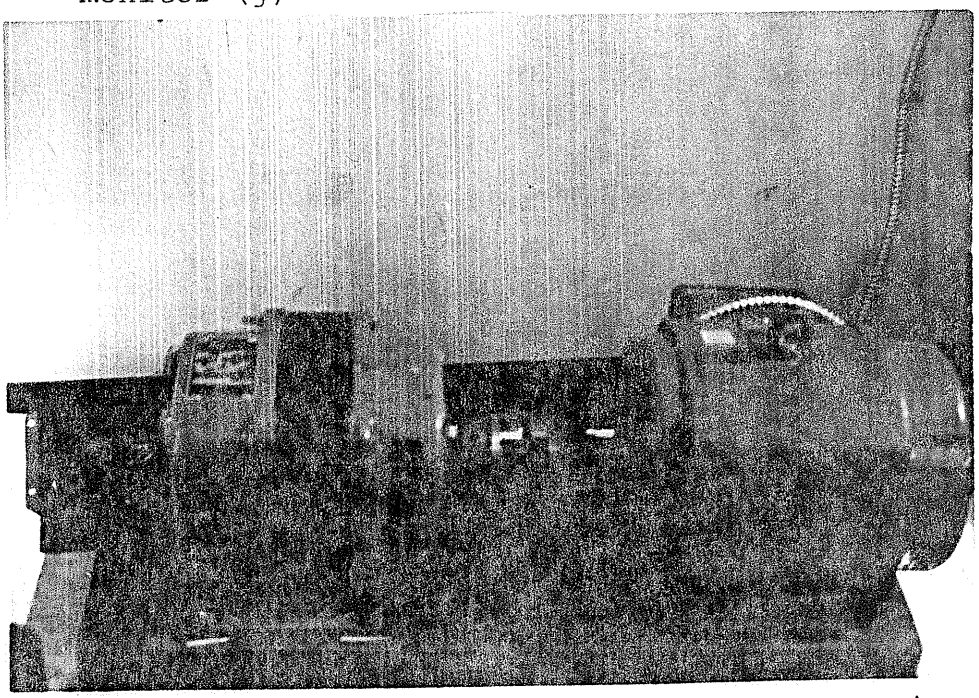

(iv) Motor-generator assembly for power generation

PLATE 2. Arrangement of AE Test Equipment

signal processor (right middle).

For calibration, another transducer was attached to the specimen through wave guide (Plate 1). A standard electric (dc) pulse from the signal generator was transmitted to the specimen and was picked up on the other side of the specimen by the sensing transducer. This pulse was preamplified to 95db gain, filtered over 0.1 to 0.4 MHz range of frequency and counted by the AE count totalizer in terms of number of counts by ring down counting mechanism. The filtered signal was also fed to biomation model, in parallel and displayed as a sinusoid signal on oscilloscope screen. The number of times the signal crossed a threshold level of 1 volt on the oscilloscope screen was counted and number matched with the counts shown by the count totalizer. In addition, the needle jump on the gradient meter of count totalizer revealed the magnitude of the standard pulse. The attenuation in the specimen and the electronic noise from the system were estimated by comparing the standard pulse with the traced signal. The system response of the standard pulse is shown in Figure 7.

Once the system was calibrated for the attenuation and the system noise under the experimental conditions, the system was ready to monitor slow crack growth. The background noise count rate was measured by putting a dummy specimen (Figure 5b) in the system and monitoring AE counts. The background count rate increased with temperature and was considerably high at temperatures about 200°C. A typical noise response with time, at different temperatures is shown in Figure 8 [51].

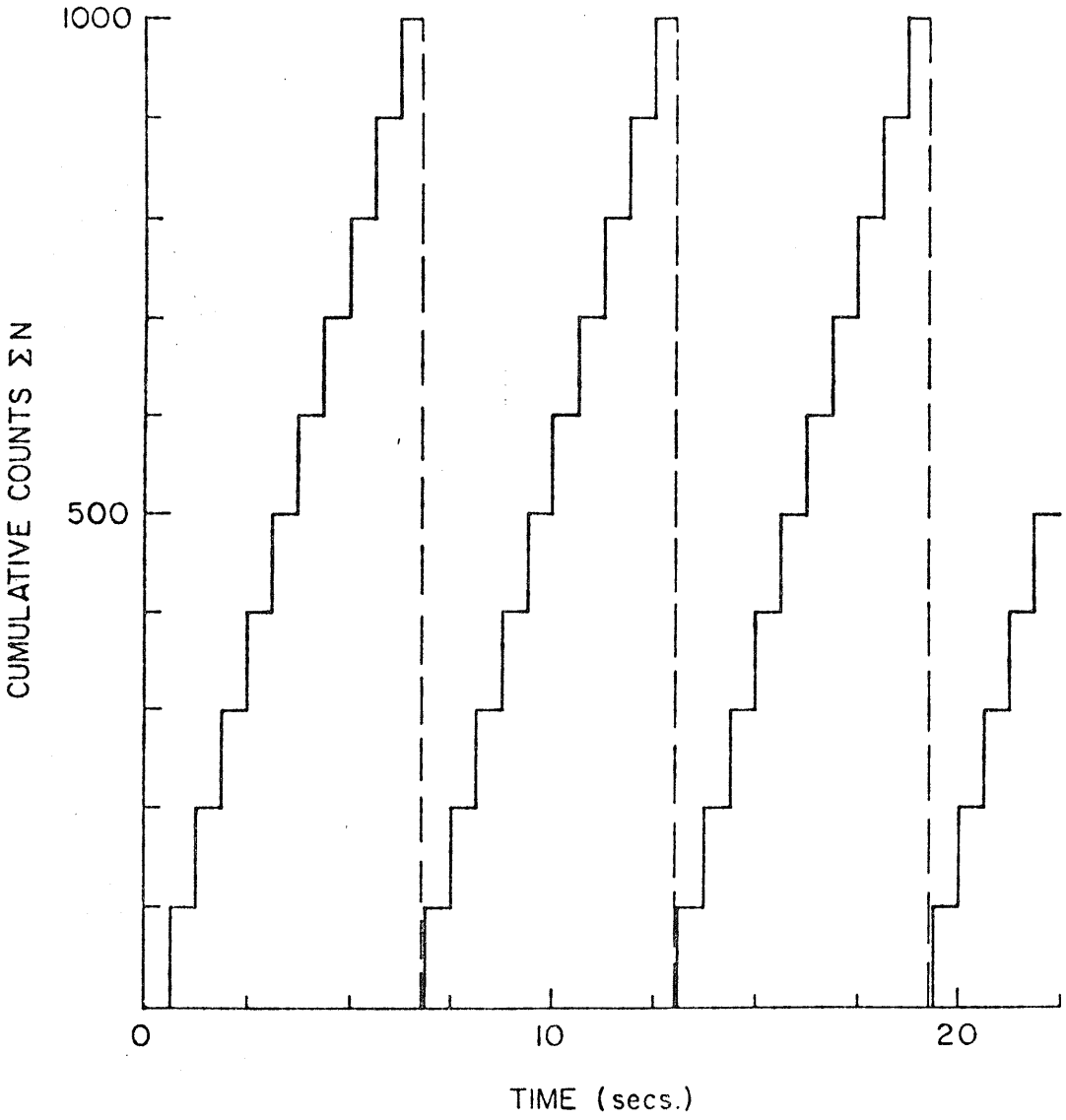

Fig. 7. Characteristic Signals of AE from System Calibration .

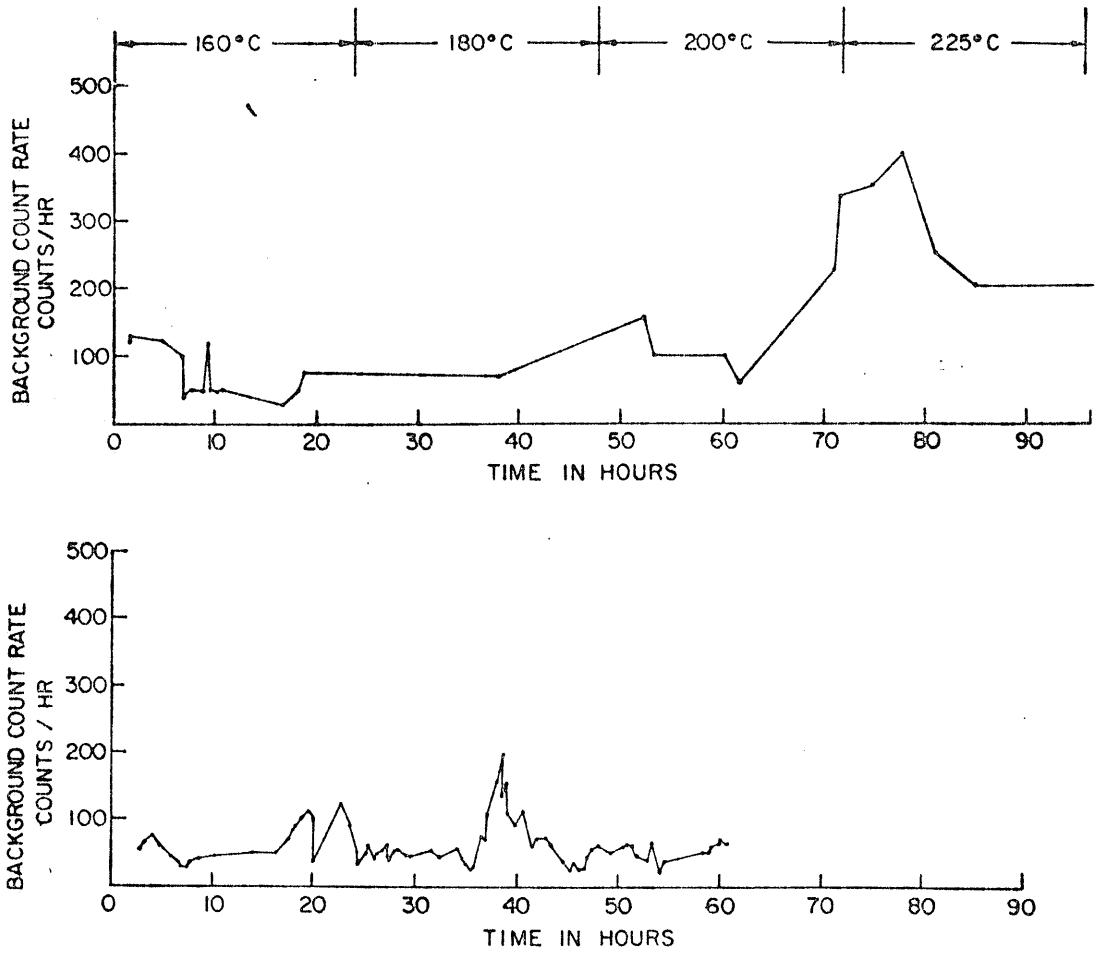

Fig. 8. Variation of Background Count Rate with Time and Temperature. Test $K_I = 20$, $MNm^{-3/2}$, Hydrogen Content 10 ppm. [51]

The system calibration for signal processor model 920 (Dunegan/Endenco, built in filter) and the AE preamplifier 802P-B (fixed gain 50 db) is explained in Appendix B.

To monitor acoustic emission from slow crack growth, the specimen was fixed in the jig, the transducer was mounted and the furnace was heated up by d.c. supply. The temperature was brought to the test temperature and maintained to ±1°C. The appropriate load, to obtain a certain crack tip stress intensity, was put on the weight pan and the acoustic emissions were monitored. The signals received by the transducer were preamplified to 95 db gain and filtered over 100 to 400 KHz frequency band pass and counted and totalized by the count totalizer and were plotted on x-y plotter against 24 hour ramp. Smaller ramps (2-4 hours) were used to observe the count rate changes preceding the bursts and just after the burst events. The AE was monitored for a sufficient length of time to analyze the AE received from cracking and slow crack growth. The test lasted as long as 700 hours in certain cases. The AE was monitored from various specimens undergoing slow crack growth under different experimental conditions of temperature and stress intensity. The temperature varied from 100-300°C while the crack tip stress intensity ranged from 5 to 20 $MNm^{-3/2}$. Some specimens were also monitored for amplitude distribution along with AE counts. The results are reported in the following chapter.

The specimens already tested for slow crack growth were reannealed at 400°C for 2 hours under vacuum and retested for different experimental conditions. Thus one specimen was used for a series of tests. The specimen was heat tinted after each test simply by raising the test temperature to 300°C and cooling the specimen in air. The fracture surface was oxidized during heat tinting and helped in measuring cracked length in each test after the fast fracture of the specimen. The fractography and metallography tests were conducted on the specimens following the AE tests.

3.5 Fractography and Metallography

The specimens were fast fractured using instron after the tests and the fracture surfaces were cleaned. These surfaces were observed at various magnifications under optical, scanning electron and transmission electron microscopes to have a better understanding of fracture process and the related mechanism of fracture.

3.5.1 Optical Microscopy

The fracture surfaces were observed under direct and oblique lighting. The salient features of the fracture surface are reported under fractography in the next chapter.

3.5.2 Scanning Electron Microscopy

The specimen was cut and mounted onto the specimen holder (1 cm diameter). The surface was coated with heavy metal (in our case gold) and observed under the scanning electron microscope at an angle of 30° from the horizontal. A

magnification of more than 1200 was employed.

3.5.3 Transmission Electron Microscopy

A two stage replica technique was used to observe the fracture surface under transmission electron microscope. The specimen was mounted in lucite and cut at the level of fracture surface (Figure 9). The mirror image of the fracture surface was received on the counter half of the lucite. This lucite surface was cleaned with a blower and shadowed with heavy metal, Cr, under vacuum at 30° from vertical. The shadowed lucite surface was then coated with carbon. The required fracture surface was then cut out from this lucite sample and was left floating in chloroform for several hours. The lucite dissolved in the chloroform and the carbon replica was left behind floating on the chloroform. This replica was fished out on 300 mesh grid, washed in fresh chloroform, acetone and distilled water respectively. The grid was put in the specimen holder and observed at 100 KV in transmission electron microscope at an angle of 35°.

3.5.4 Metallography

Metallographic examinations were conducted on the hybrided and unhydrided specimens to determine the particle size and to study its distribution and orientation. The growing crack and other surface effects like shear lip, crack tunnelling, etc. were observed. Some specimens were surface etched to show the hydride precipitation adjacent to or ahead of the growing crack tip.

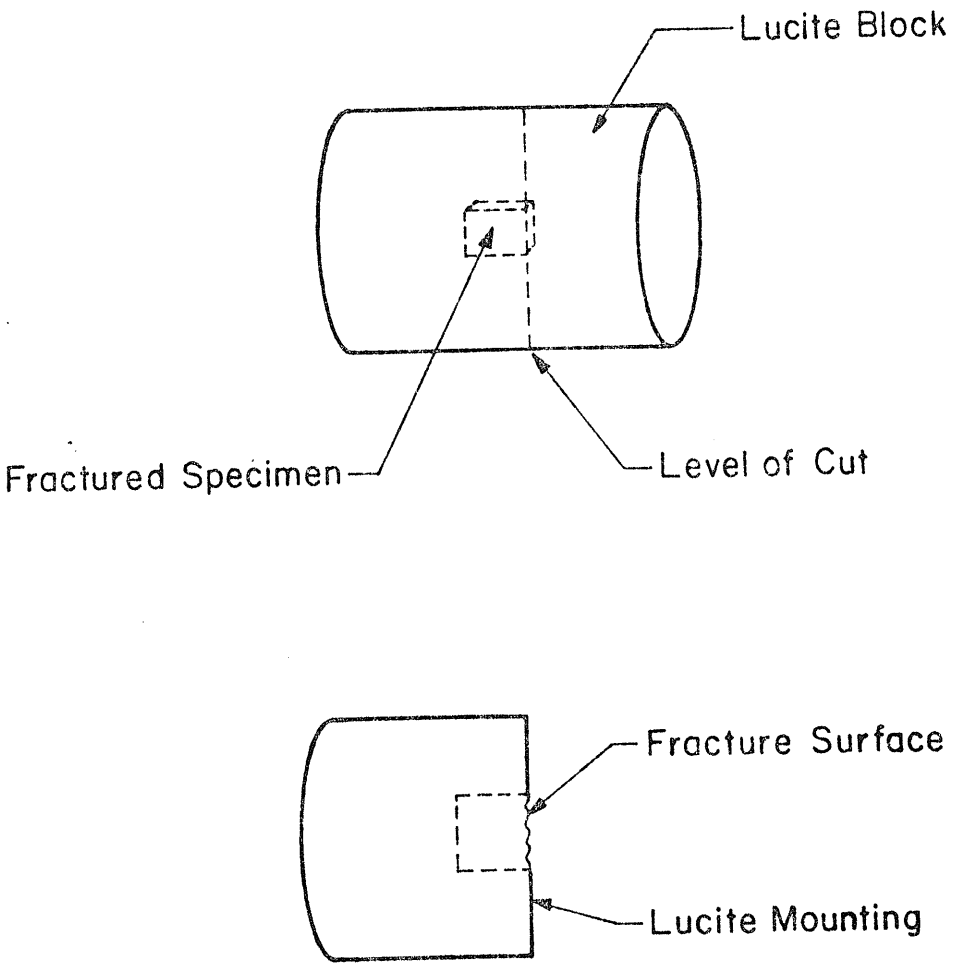

Fig. 9. Fractured Specimen Mounted in Lucite and Cut at the Level of Fracture Surface .

4. RESULTS

The acoustic signals have been characterized and the AE results have been interpreted on the suggested models of cracking and crack growth in Zr-2.5% Nb. It has been established that the diffusion of hydrogen under the conditions of elevated temperature and stress occurs towards the crack tip and the preci pitation of hydride takes place in the plastic zone or at elastic-plastic boundary. The crack under high crack tip stress intensity ploughs through the precipitated brittle hydrides and is arrested in the Zr matrix. It is assumed here that the brittle hydride cracking produces big acoustic signal whereas the Zr matrix being ductile produces only small continuous signals. Some amount of AE is also produced during plastic deformation, however, it is quite small compared to the AE signal from cracking of brittle hydride particles.

4.1 Signal Characterization and Signal Analysis

A number of preliminary experiments were conducted on CT specimens for monitoring AE during cracking and crack growth. The results provided information concerning the nature of acoustic emission and the repeatability of the AE data. Mainly three types of signals were observed during AE monitoring (i) big burst type, (ii) small continuous type, (iii) transient type. These signals are shown in Plate 3. The big burst type signals were believed to come from crack growth, for the reason that there will be a relatively large

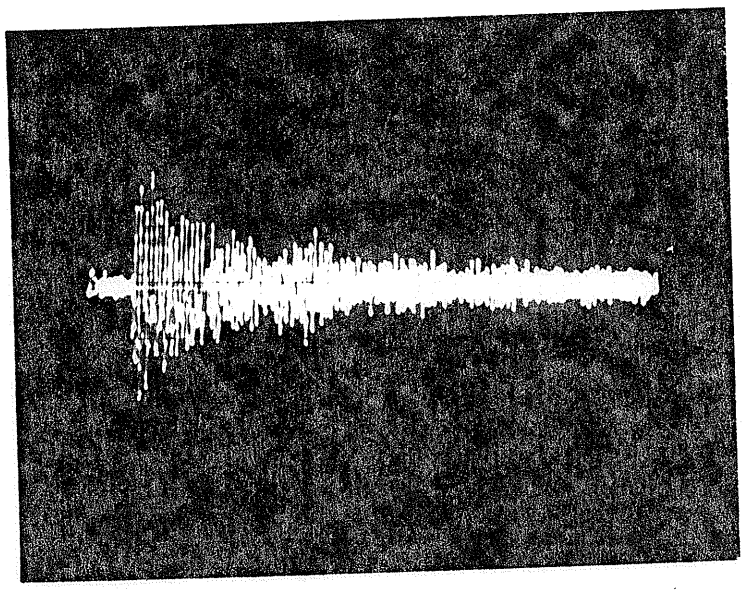

(a) Big burst signal

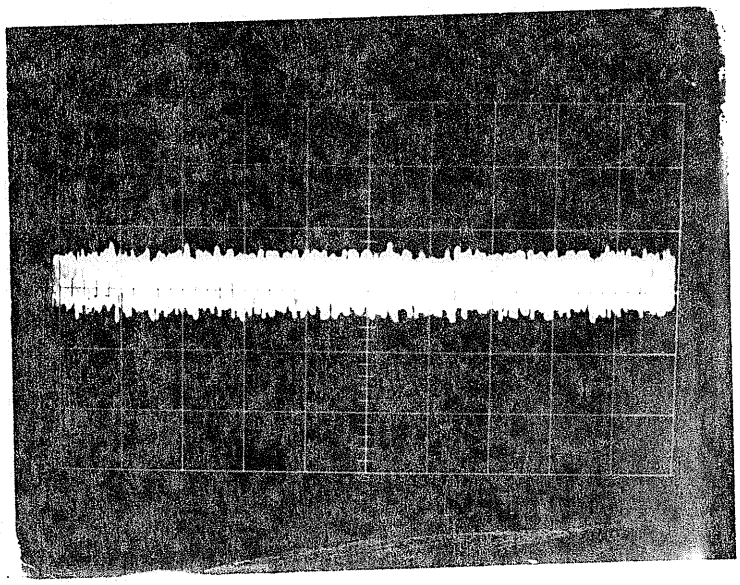

(b) Small continuous signal

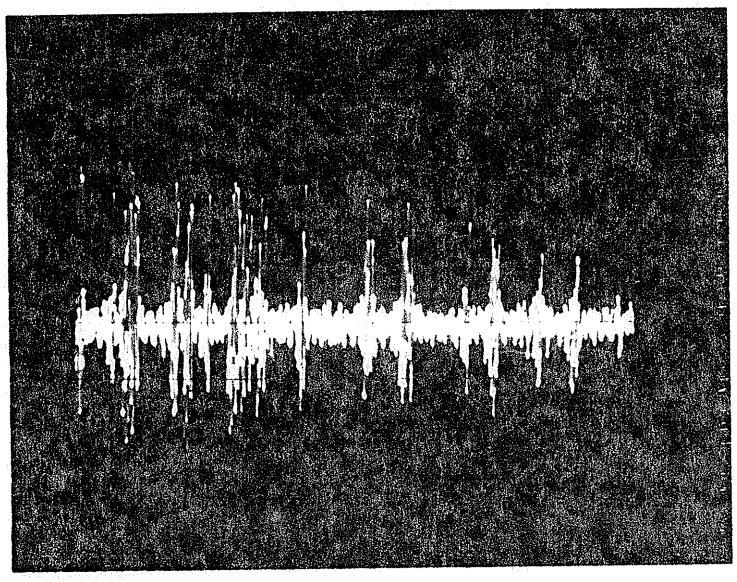

(c) Transient signal

PLATE 3. AE Signals Received From Test Set-Up

energy release during cracking compared to uniform plastic flow which would result in small continuous-signal. Some amount of continuous signals also emanated from system noise, i.e. electronic, equipmental or environmental. The transient signals were the result of line or building transients which affected the system. The transient signals from ambient were trapped by faraday cage and were not monitored during the test. The terminology used in AE studies is defined in Appendix C.

A dummy sample (Fig. 5b) was used to determine the background noise level. The temperature was maintained at 126°C and the noise count rate was established at different hours of the day. The background count rate was also determined at different temperatures in the range of 160 to 225°C. Fig. 8 shows how the background count rate varies with time and temperature. Once background noise level was known, the pre-fatique-cracked CT specimens were tested for Acoustic Emission response. The dimensions, loads required for the test K_I and test conditions for all the specimens are reported in Table 2. Acoustic Emissions were continuously monitored for extended period, up to 700 hours in certain cases. A typical segment of an AE plot (ΣN vs time) is given in Fig. 10, which shows sharp burst signals of varying magnitude randomly spaced in time. The sharp burst signals were captured by biomation system and displayed on an oscilloscope screen. The large bursts in the plot (IIa, Fig.10) correspond to big burst signals (Plate 4a) and the small bursts (IIb, c, Fig. 10)

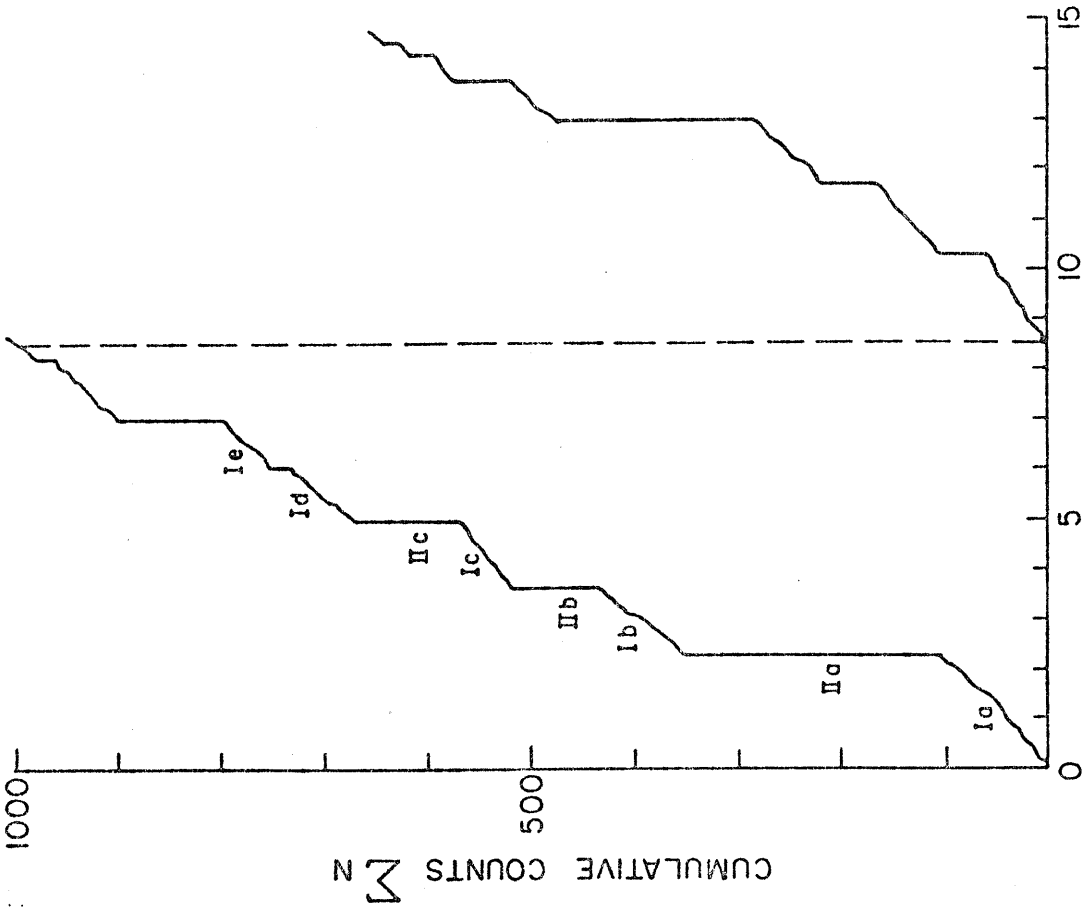

Fig. 10. A Typical Segment of ΣN vs. Time Plot.

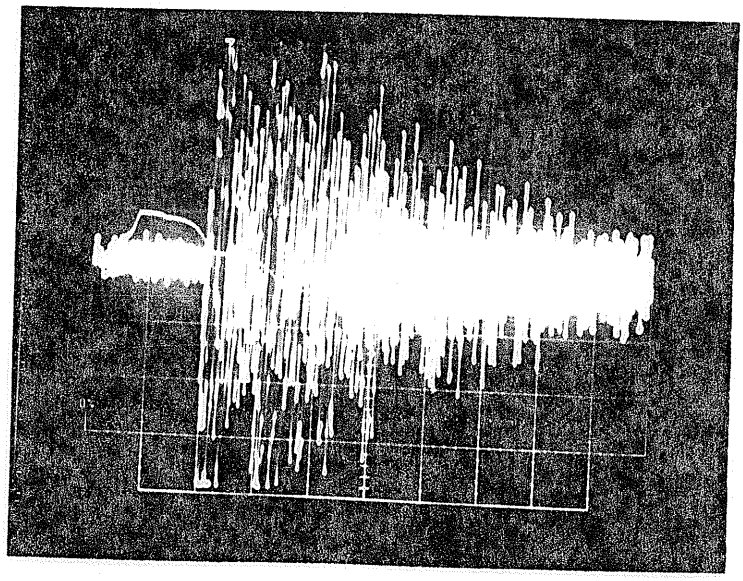

(a) Large burst signal

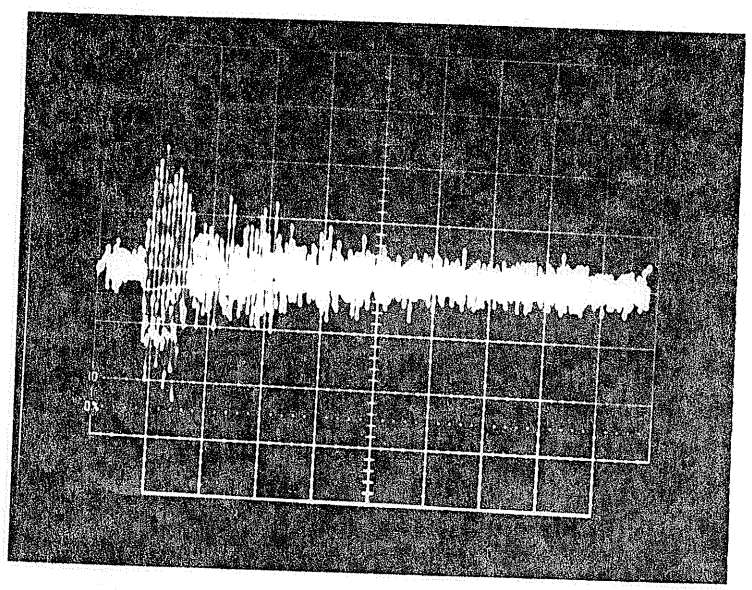

(b) Small burst signal

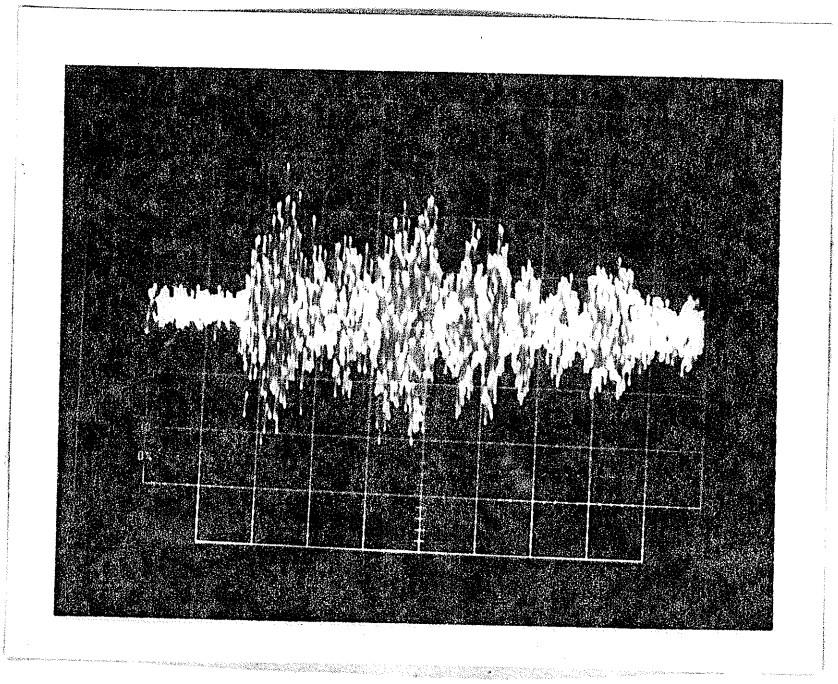

(c) Over-riding signals

PLATE 4. Characteristic Burst Signals from Slow Crack Growth

Table 2

Specimen No.	a in.	W in.	b in.	$(b \cdot W^{1/2})$	Selected K_I $MNm^{-3/2}$ / $lbs/in^{3/2}$	(a/w)	f(a/w)	$P_{lbs} = \frac{K_I x (b \cdot W)^{1/2}}{f(a/w)}$	Test Temp. C	Test Time hrs.	Crack Length lo mm	Hydrogen Content ppm	Comments
#A1	0.6203	1.344	0.146	0.1693	19/17287.25	0.4615	8.606	340.00	140	400	2.70	10	SCG test
#A2A	0.6734	1.344	0.144	0.1669	19/17287.25	0.5010	9.630	300.00	140-185	606	4.05	10	effect of temperature
#A2B	0.6734	1.344	0.144	0.1669	19/17287.25	0.5010	9.630	300.00	100	139	4.05	10	fast activity & aging test
#A3	0.6122	1.344	0.145	0.1681	19/17287.25	0.4555	8.510	341.50	100	212	2.55	200	stress-aging (60 hrs) test
#A4	0.6233	1.350	0.142	0.1650	19/17287.25	0.4617	8.606	331.44	100	145	2.70	200	stress-aging (40 hrs) and K_I test
#A5	0.6200	1.345	0.145	0.1681	19/17287.25	0.4610	8.595	338.22	100	270	2.53	200	stress-aging (20 hrs) test
#A6	0.6075	1.345	0.143	0.1658	19/17287.25 + 10-20	0.4517	8.377	342.22	100	144	2.45	200	SCG test + K_I vs. IP & fast activity
#A7	0.5842	1.313	0.135	0.1547	19/17287.25	0.4450	8.230	324.29	100	256	1.30	10	stress-aging (40 hrs) test
#A8	0.5650	1.341	0.145	0.1682	19/17287.25 + 5-10-15	0.4197	7.704	377.44	140	370	1.20	200	SCG test + K_I vs IP & fast activity

correspond to small burst signals (Plate 4b). Some overriding burst signals (Plate 4c) also produced big bursts in the ΣN-time plot. The incubation period (Ia, Fig.10) varied from test to test and was of the order of interburst period (Ib, c, Fig. 10).

A histogram of the bursts (cracking events) for the first test (#A1) is shown in Fig. 11. The frequency of occurance of cracking events can be noted with time. The burst events on the onset of loading occur very fast and slow down with time. The detailed analysis of bursts, incubation period and interburst period is carried out in #4.2. An average AE count rate throughout the test was 40-50 counts/ hour.

The specimens were tested in stage II of V-K curve over a temperature range of 100-225°C for a period of 10 to 15 days on the average. The ΣN vs time plots for the duration of the tests were recorded and the data analyzed. Since the bursts correspond to the crack growth, the main interest lay in analyzing the bursts. In attempts to extract information from ΣN-time plot about the signals corresponding to the cracking, the counts in each burst were measured and tabulated. One of the sample tables is shown in Table 3. Then the data from such table were plotted. A typical plot is shown in Figure 12. The plot consists of three regions; (i) an incubation period, (ii) the fast activity, and (iii) the stabilized AE.

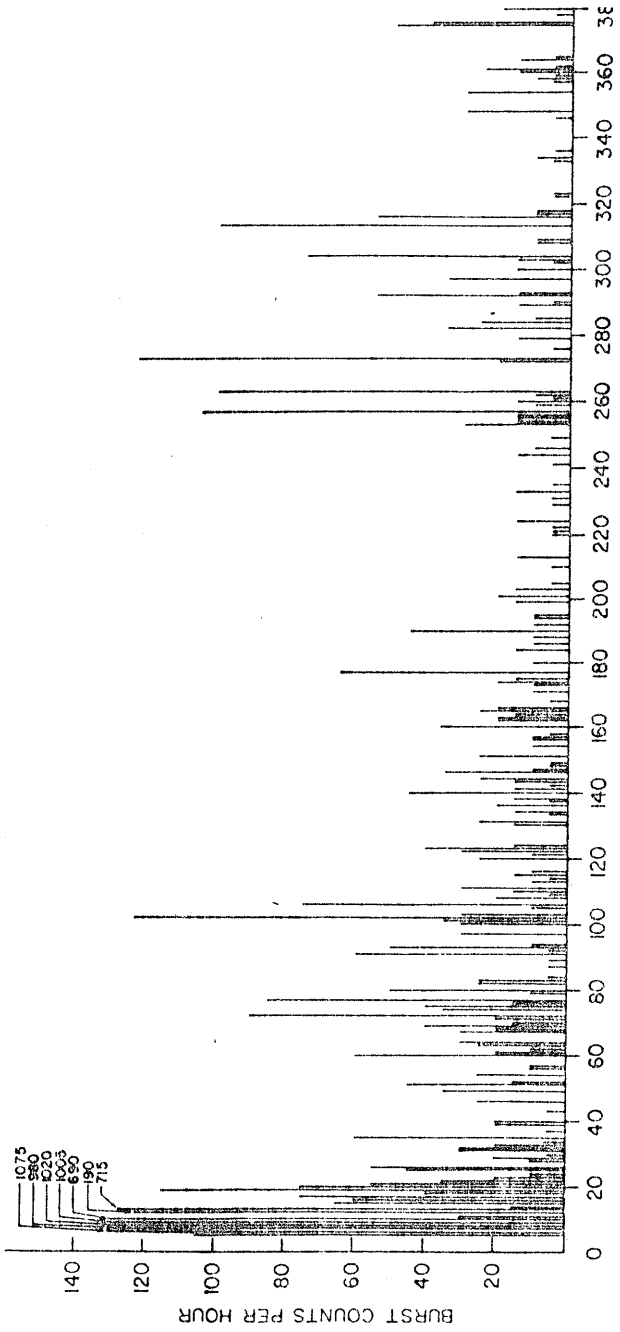

Fig. 11. Histogram of Burst Counts Per Hour for Specimen # A1 .

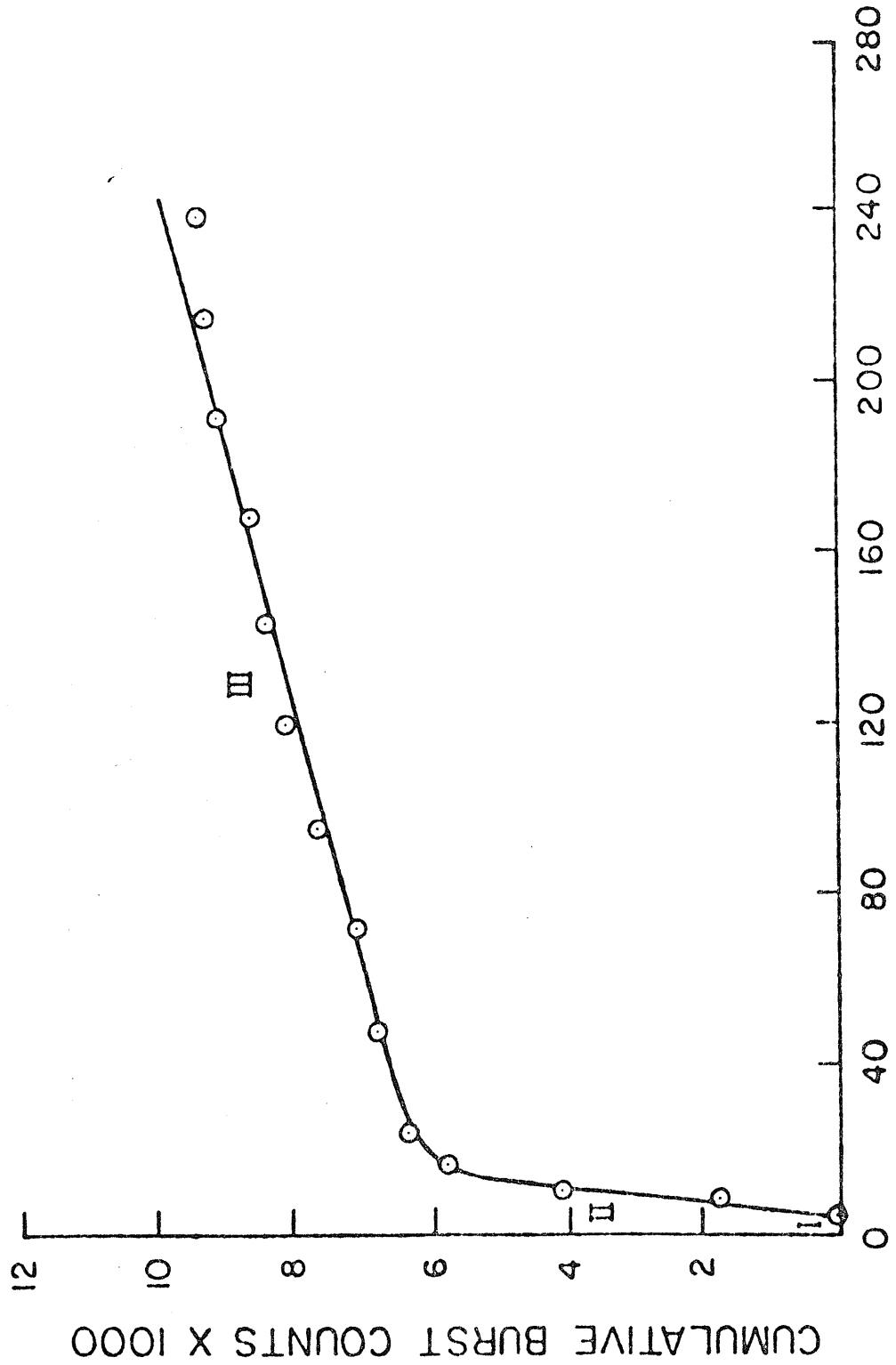

Fig.12. Cumulative Burst Counts vs. Time. Test Temperature 140°C, Hydrogen Content 10 ppm.

Table 3

Hour No.	Event/hr.	Counts per event	Counts per hour	Total Counts	Comments
1	3	250,25,25	300	300	
2	3	15,125,20	160	460	
3	2	15, 5	20	480	
4	1	10	10	490	
5	1	5	5	495	
6	2	10, 5	15	510	
7	2	25, 55	80	590	
-	-	-	-	-	
-	-	-	-	-	
-	-	-	-	-	

4.2 Effect of Stress Intensity, Temperature and Hydrogen Content

4.2.1 On Incubation Period and Fast Activity

The incubation time is the time required for cracking to initiate. The crack-incubation time depends on the rate of hydrogen diffusion and its precipitation ahead of the crack tip. To study the effect of stress intensity on the incubation period, supplementary tests were conducted. Specimen #A6 and #A8 were tested at 100°C and K_I = 5, 10, 15 and 19 $MNm^{-3/2}$, respectively and AE monitored. Each time the specimen was unloaded, it was stress relieved, and then reloaded to next K_I value. It was observed that the incubation

period decreased with the increase in crack tip stress intensity (Fig.13). The temperature did not have any significant effect on the incubation period. The second region, i.e. the fast activity, arises from the fast (and multiple) fracture of the accumulated hydride particles. The accumulation of hydrides occurs adjacent to the crack tip (in the plastic zone and at elastic-plastic boundary) during the incubation period, since the pre-existing particles assist the hydride precipitation and the particle growth. The fast activity rate and the length of this period varied considerably in the experiments. The increase in stress intensity produced an increase in the fast activity rate and the absence of incubation period reduced the fast activity region. With an aim to reach to region III by avoiding fast activity, attempts were made to reduce incubation period, and in view of above, experiments were conducted on specimens, employing a stress-aging treatment. A detailed discussion is presented in Section 4.3.

4.2.2 On Stabilized AE

The stabilized AE in region III corresponds to stable slow crack growth. Since the burst height represents a crack increment and the burst count rate in this region should be a measure of crack growth rate. AE were monitored for long periods to observe any variations in the AE count rate in this region. A linear relationship was observed between burst counts and time (Fig. 12). The average burst count rate at 140°C and at a crack tip stress intensity of

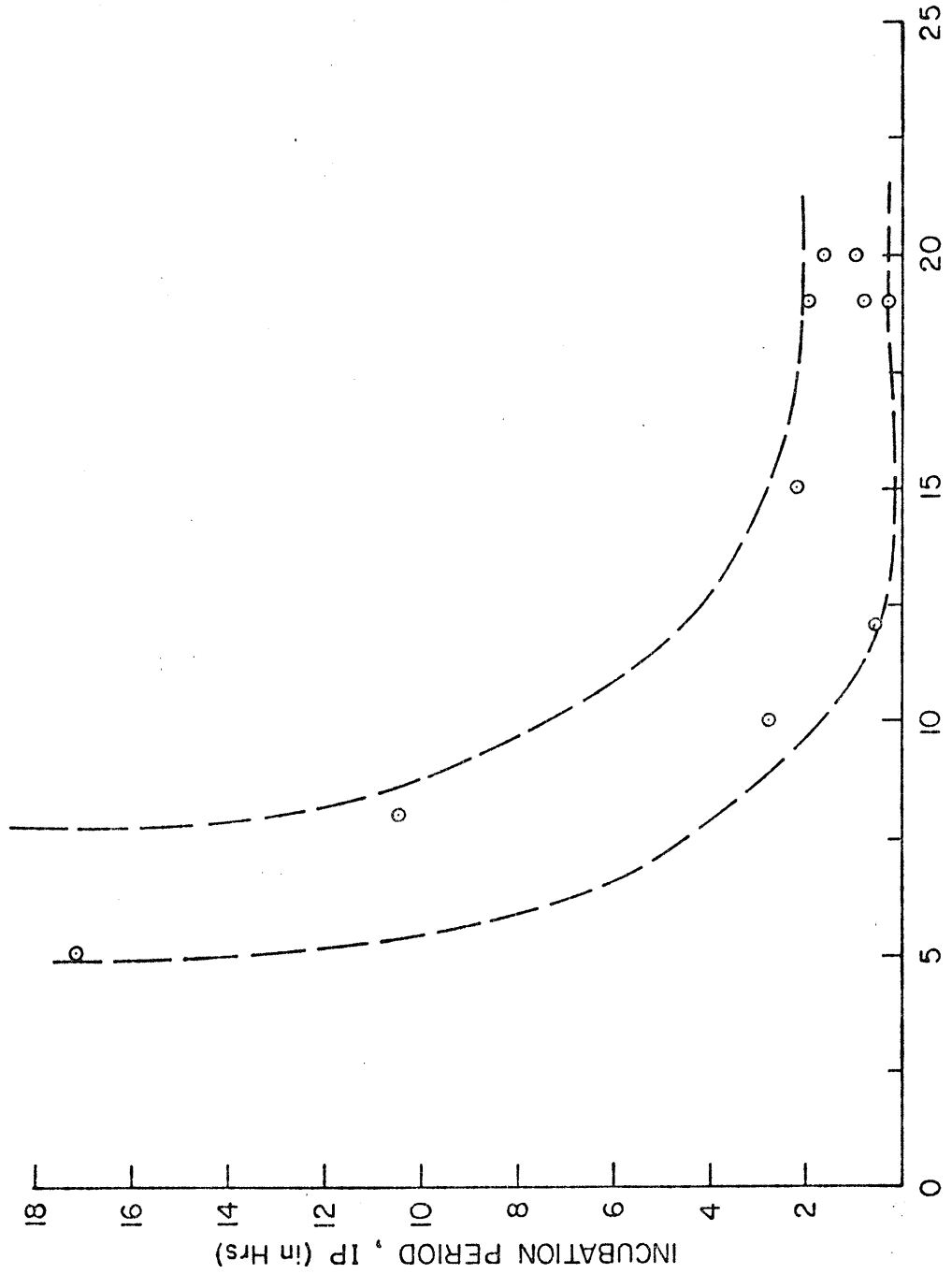

Fig. 13. Incubation Period vs. Crack Tip Stress Intensity

19 $MNm^{-3/2}$ was between 20-30 counts/hour.

To study the effect of temperature on the acoustic emission response of slow crack growth (SCG), two types of experiments were conducted. First, the CT specimens were tested at certain fixed temperatures for a long time and the burst count rates measured. Two specimens, #A3 and #A4, were tested at K_I of 19 $MNm^{-3/2}$ and 100 and 140°C, respectively. The AE results showed essentially the same AE rates (Fig. 14). In the second experiment, a specimen (#A2A) was loaded to a K_I value of 19 $MNm^{-3/2}$ and the temperature was raised from 140°C in steps of 3 to 5°C. AE was monitored at each temperature for 1 to 2 days. It was observed that the AE signals reduced considerably above 160°C and was absent above 185°C. In another test to confirm the effect of higher temperatures (>140°C), AE monitoring revealed that the frequency of AE bursts decreases with increase in temperature and no bursts occur above 200°C. A histogram of bursts with time is given in Fig. 15. The fractographic studies confirmed that there was no crack growth above these temperatures (discussion in Section 4.4).

The effect of hydrogen content on AE response of SCG was studied on specimens #A1 and #A8, at a constant K_I of 19 $MNm^{-3/2}$ and at 140°C. Specimen #A1B contained 10 ppm hydrogen while specimen #A8B was hydrided and contained 200 ppm hydrogen. The results are given in Fig. 16. In fast activity region, AE rates were not significantly different, however the stable AE rate varied from 15 counts/hour for unhydrided specimen

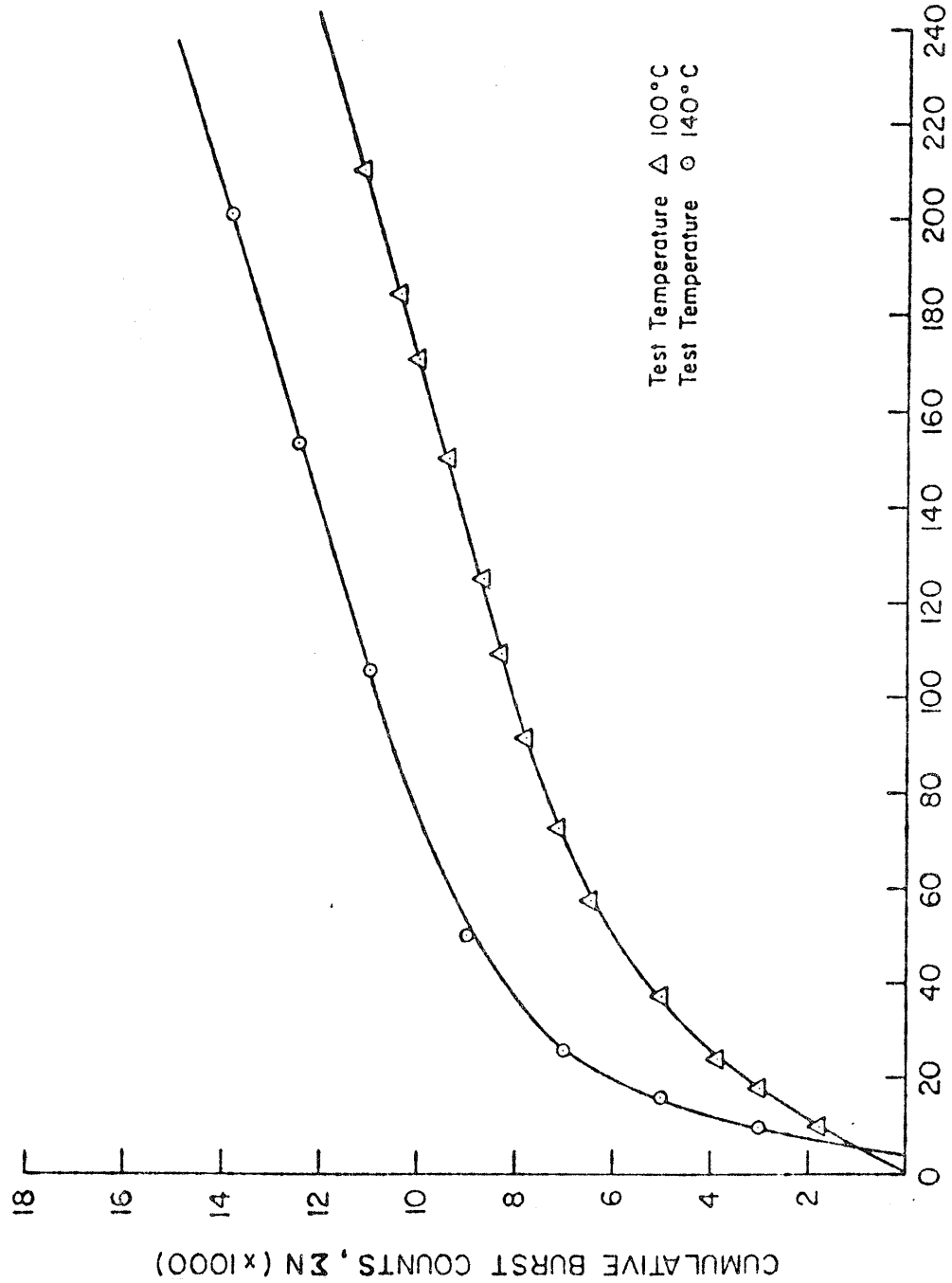

Fig. 14. Effect of Temperature on AE Response of Slow Crack Growth. Hydrogen Content - 200 PPM. Test $K_I = 19\ MN_m^{-3/2}$.

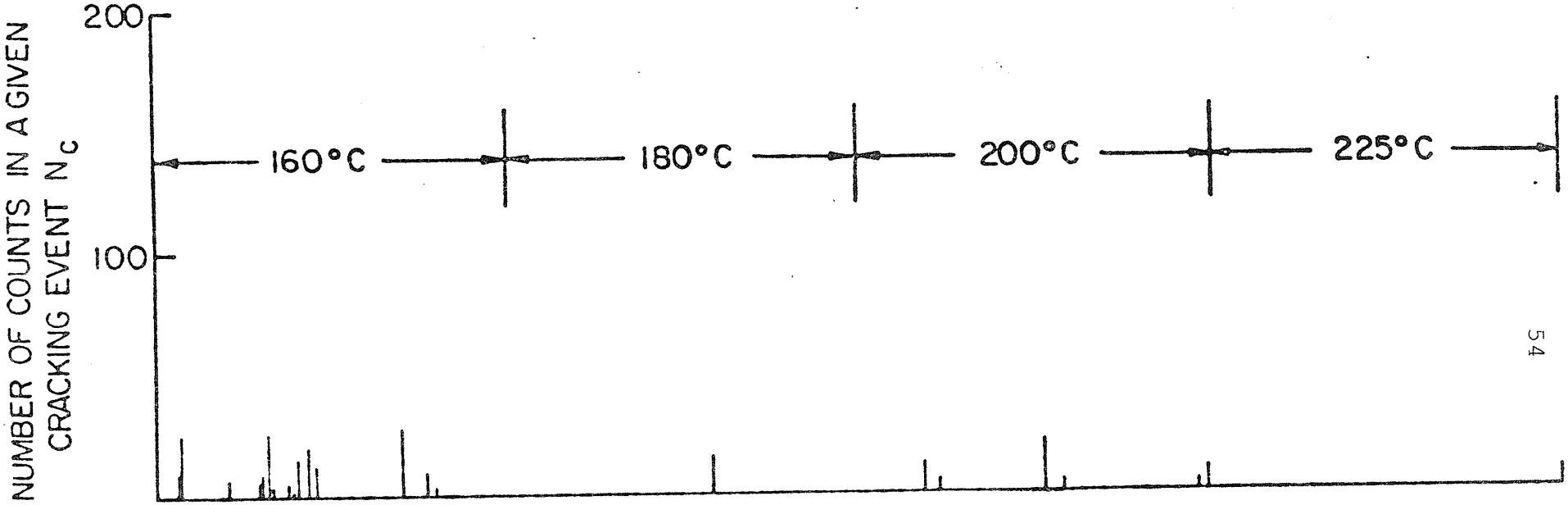

Fig.15. EFFECT OF TEMPERATURE ON AE ACTIVITY

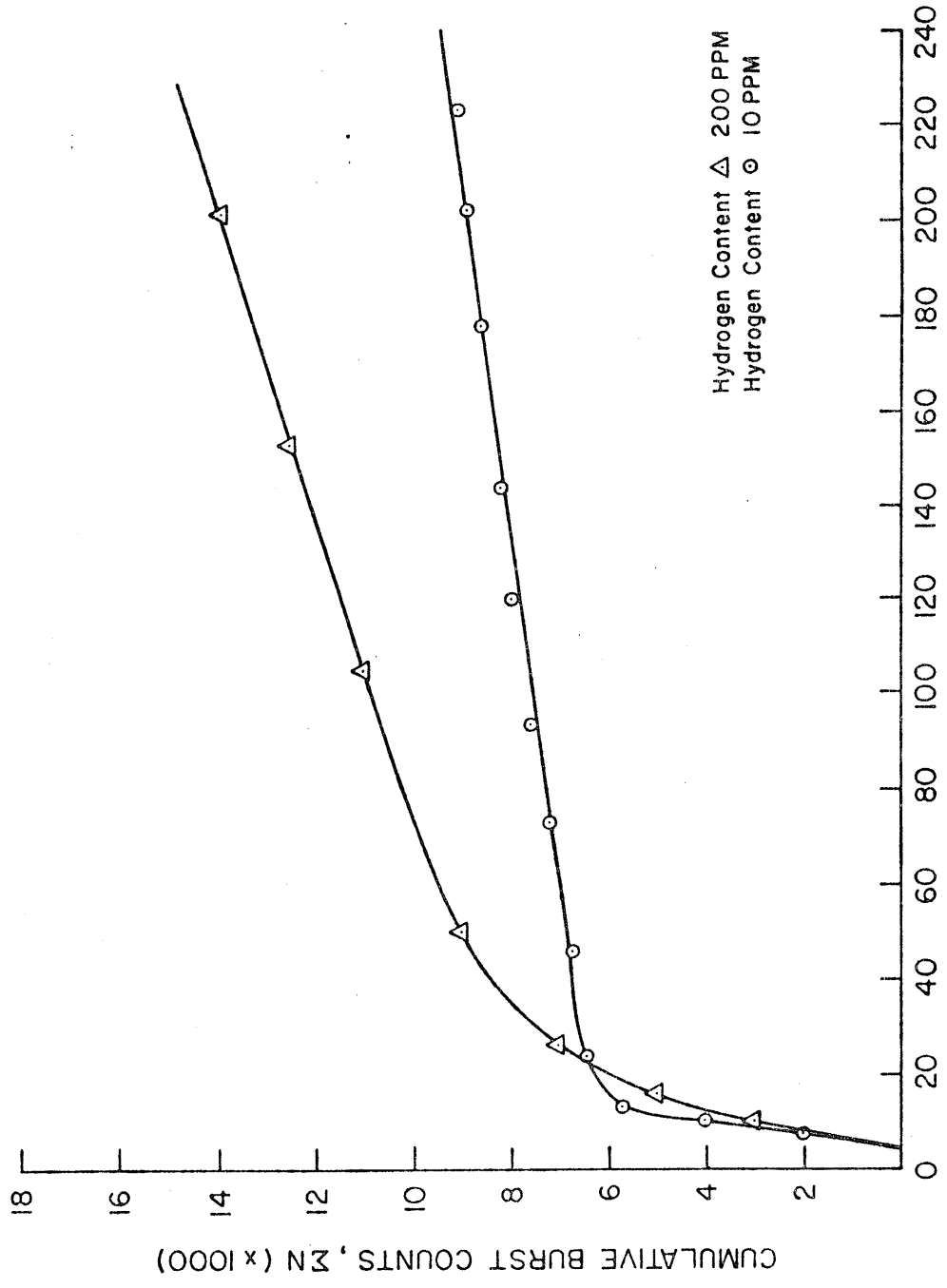

Fig.16. Effect of Hydrogen Content on AE Response of Slow Crack Growth. Test Temperature 140°C. Test $K_I = 19 MN_m^{-3/2}$.

to 30 counts/hour for hydrided specimen. Later metallographically it was found that the crack velocity in hydrided specimen was also approximately twice of that in unhydrided specimen (Table 4).

The specimens, which were already tested for AE response of SCG under different experimental conditions, were fast fractured. The area swept by the crack during SCG was measured and the results were computed (Table 4).

Table 4

Specimen No.	Cumu. Burst Counts ΣN	Area Cracked $\Delta A (mm^2)$	N/A $(x10^4)$	Test Time t(sec) $(x10^4)$	Crack Extension $\Delta \ell$ (mm)	Crack Velocity v(m/sec)	Count rate $\dot{N}$ $(x10^{-2})$
#A1	10,760	1.4834	0.72	144.00	0.40	$2.78x10^{-10}$	0.75
A2A	23,100	2.1946	1.05	218.16	0.60	$2.75x10^{-10}$	1.06
A2B	27,690	3.1090	0.89	50.04	0.585	$1.70x10^{-9}$	5.53
A3	16,880	1.8415	0.92	76.32	0.50	$6.55x10^{-10}$	2.21
A4	1,610	0.3607	0.45	39.60	0.10	$2.52x10^{-10}$	0.41
A5	3,000	1.0312	0.29	97.20	0.28	$2.88x10^{-10}$	0.31
A6	6,600	0.9081	0.73	51.84	0.25	$4.82x10^{-10}$	1.27
A7	4,810	0.5144	0.93	56.16	0.15	$2.67x10^{-10}$	0.86
A8	27,000	2.7623	0.98	133.2	0.75	$5.63x10^{-10}$	2.03

It was observed that the crack velocity was of the order of 10^{-10} m/sec except for one specimen (#A2B). The AE burst count rate was of the order of 10^{-2} counts/sec and could be used to determine the crack velocity in terms of burst count rate. A plot between crack velocity and burst count rate is

given in Fig. 17. Table 4 shows that a number of burst count per unit area swept by the crack is within the range of (0.29-1.05) x 10^4 counts/mm^2 with an average of 0.77 x 10^4 counts/mm^2. Fig. 18 shows the variation of burst count with the area cracked during SCG. It may be noted that cumulative burst count (ΣN) is in direct proportionality with the area cracked (ΔA).

4.3 Effect of Thermomechanical Treatment on AE

A thermomechanical treatment was employed to suppress the incubation and fast activity period observed in earlier experiments. The CT specimens were initially subjected to stress-aging treatment at 100°C under K_I 0f 2.5 $MNm^{-3/2}$ for 20 to 60 hours. Subsequently slow crack growth studies were made on these specimens at 100 and 140°C and K_I of 19 $MNm^{-3/2}$. The stress-aging treatment suppressed the initial fast activity (Fig. 19). In this specific instance the fast activity rate reduced 630 counts per hour to 370 counts per hour. A log-log plot of AE cumulative burst counts against time presented in Fig. 20, indicates an order of magnitude reduction in fast AE activity by stress-aging treatment. The beneficial effects of this treatment was also observed in region III. Fig. 21 shows how the AE count rate is brought down by prolonged stress-aging treatment given to specimens before slow crack growth tests. Typically, for a 60 hour treatment at 100°C and K_I of 2.5 $MNm^{-3/2}$, the AE rate was reduced to about 3 counts per hour. An increased amount of coarsened hydride particles was observed on stress-aged specimen surface during metallographic

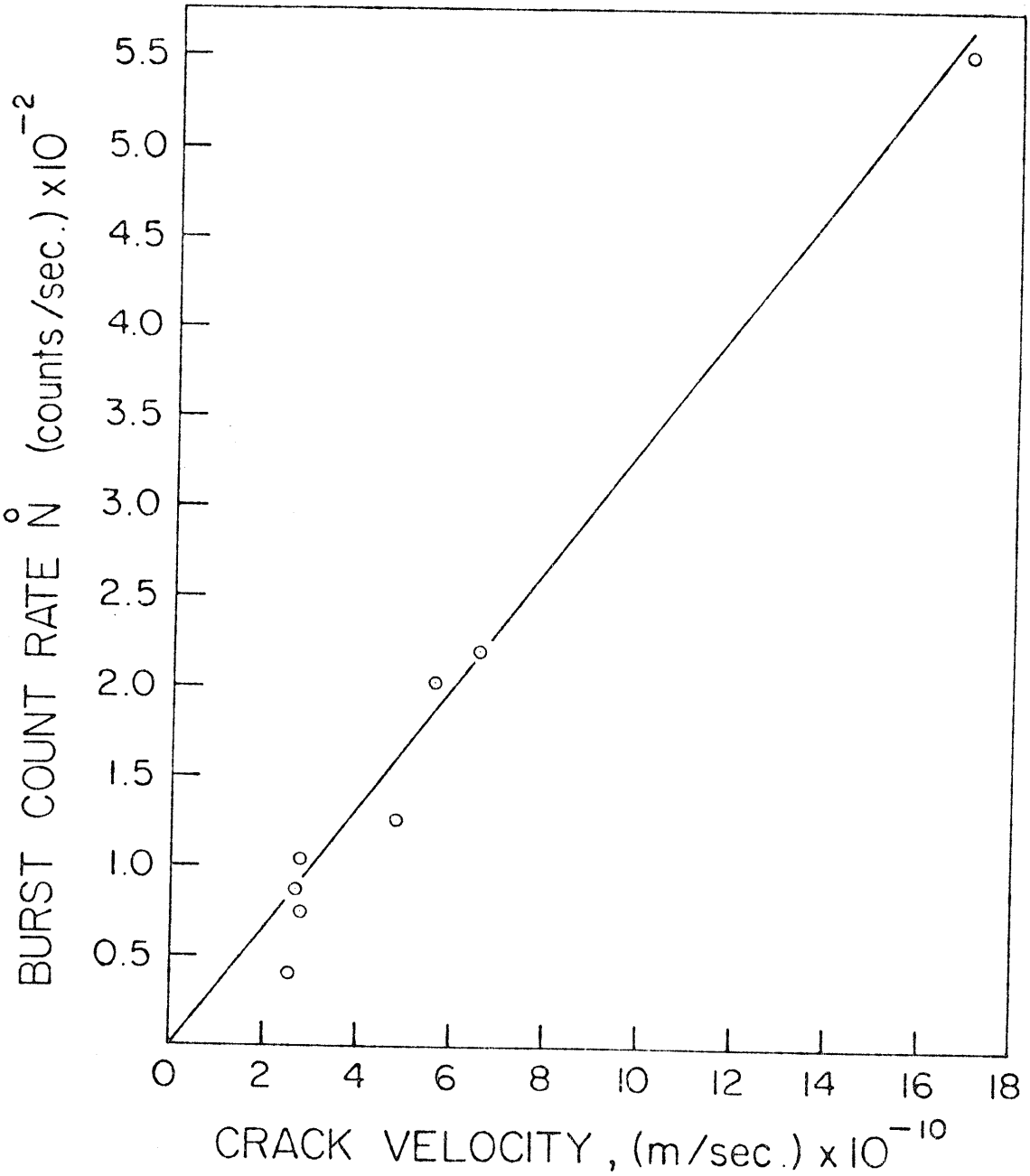

Fig. 17. Burst Count Rate vs. Crack Velocity

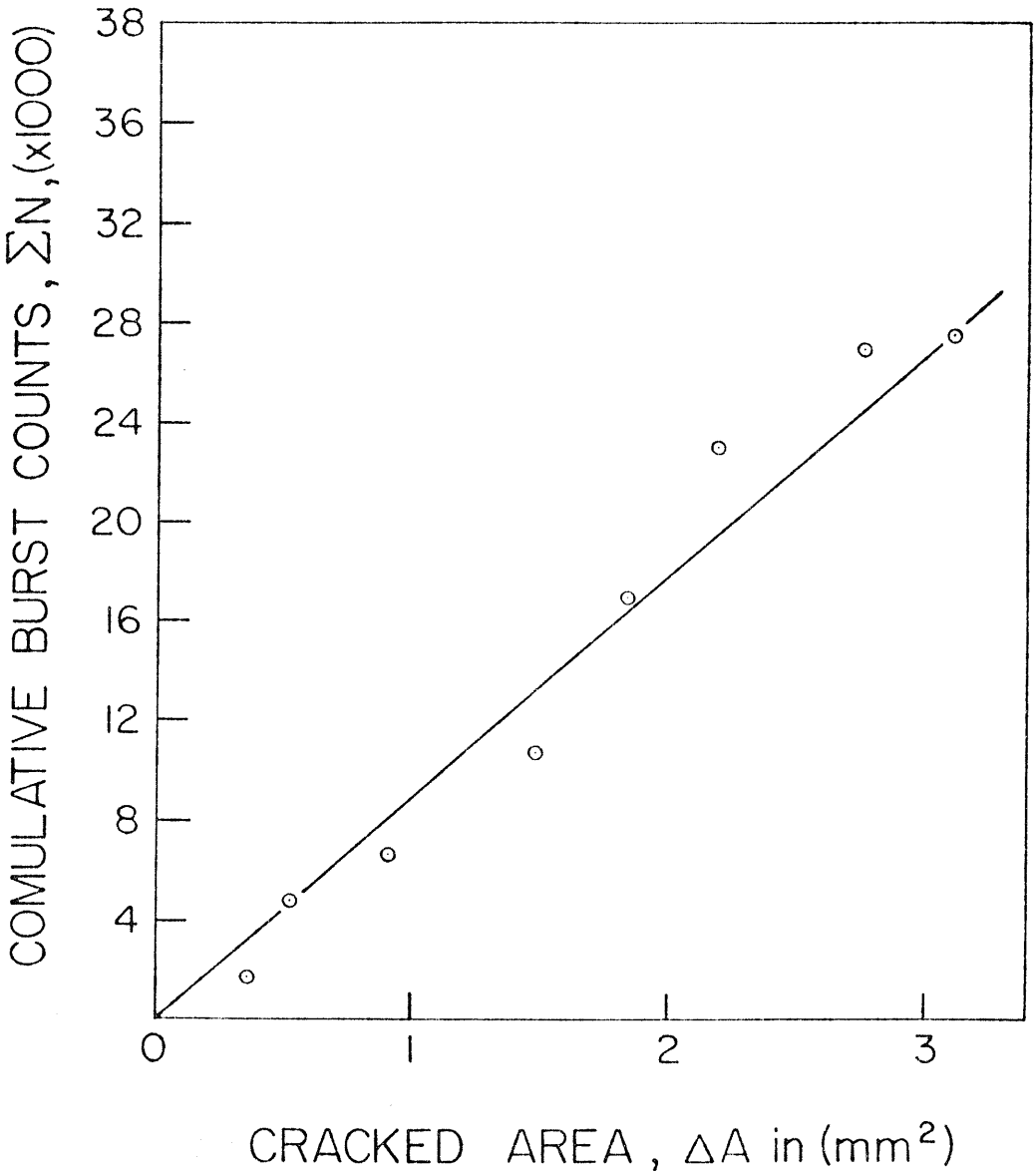

Fig. 18. Comulative Burst Counts vs. Cracked Area.

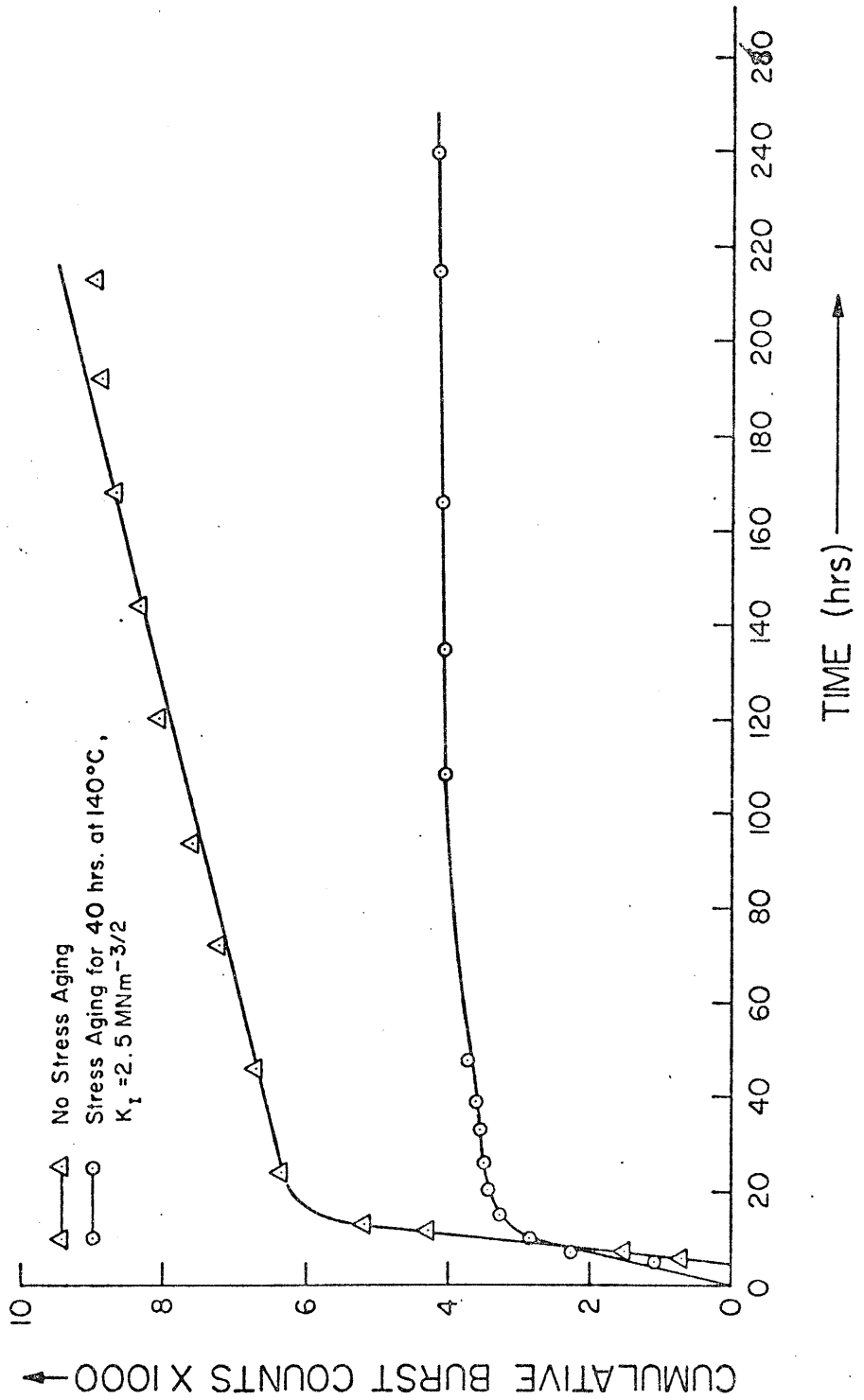

Fig. 19. Effect of Stress Aging on Acoustic Response of Slow Crack Growth in Unhydrided Specimen. Test Temp. 140°C, K_I=19 MNm$^{-3/2}$

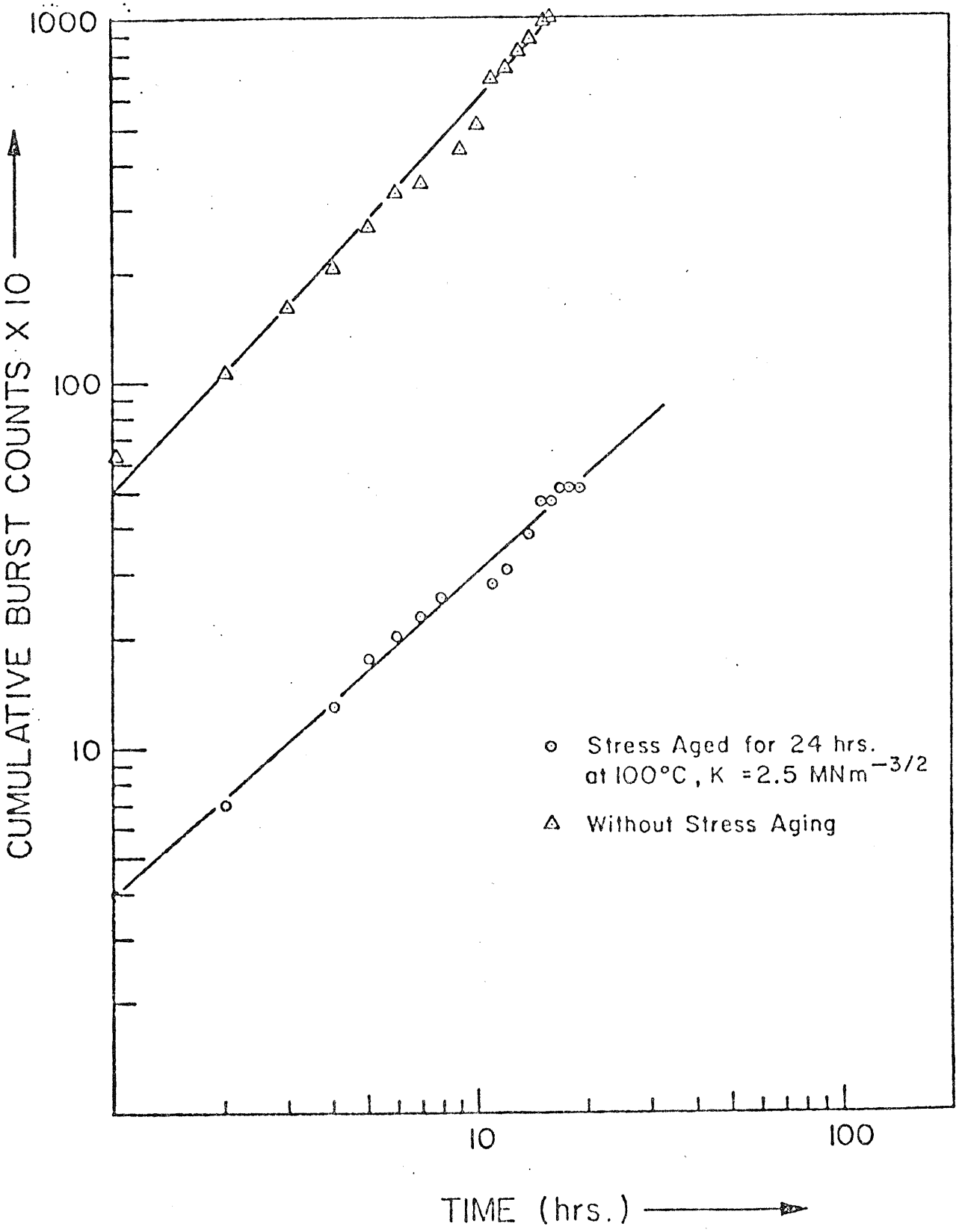

Fig. 20. Effect of Stress Aging on AE Response of Crack Growth Test Temp. =100°C ; K_I =19 MNm$^{-3/2}$

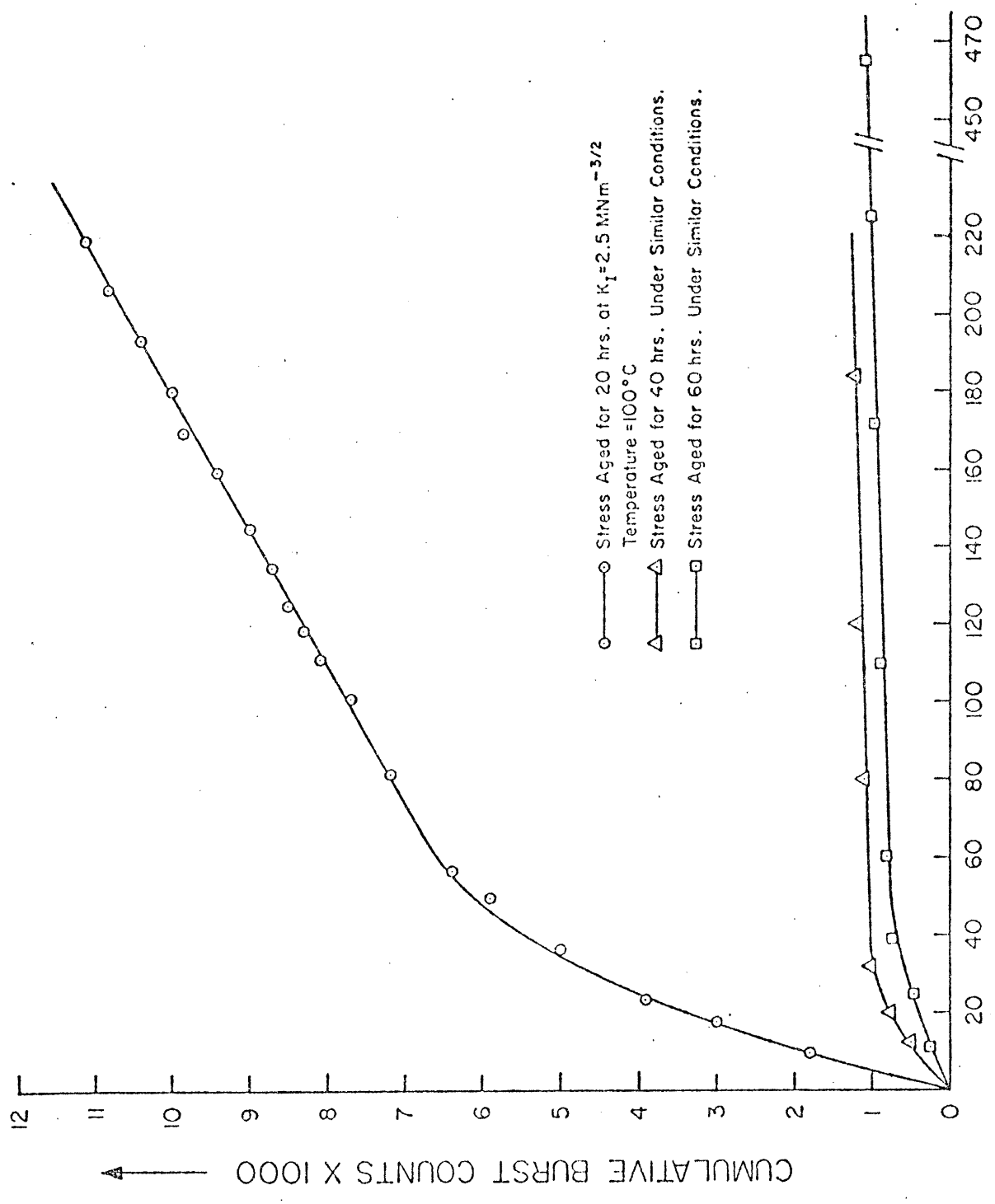

Fig.21. Effect of Stress Aging on Slow Crack Growth. Test Temp.100°C, K_I=19 MNm$^{-3/2}$
Hydrogen Content =200 ppm .

examinations.

Other results of SCG in stress aged, hydrided and unhydrided specimens are shown in Table 5. It was observed that in all regions (i) prolonged stress aging treatments suppresses the AE count rate more effectively and (ii) stress-aging reduces AE activity more effectively in hydrided samples than unhydrided sample.

Table 5

Specimen No.	Hydrogen Content ppm	Test Temp. °C	Duration of stress-aging hrs	fast activity count rate without treatment	fast activity count rate with treatment	Reduction ratio
#A7	10	140	40	630	370	0.59
#A5	200	100	20	148	110	0.74
#A4	200	100	40	148	30	0.20
#A3	200	100	60	148	18	0.12

For specimens with higher hydrogen content, the stress aging had more pronounced effect. Fig. 23 shows the AE counts with time for unhydrided and hydrided specimens containing 10 and 200 ppm hydrogen respectively.

To study the effect of incremental rise in stress intensity value on the course of AE activity, a stress-aged specimen (#A4, stress aged at K_I = 2.5 $MNm^{-3/2}$ and 100 °C) was employed. AE activity vertually ceased after 130 hours (Fig. 22). The state of inactivity continued even when K_I was raised to 20 and 21 $MNm^{-3/2}$ and maintained for 24 hours at

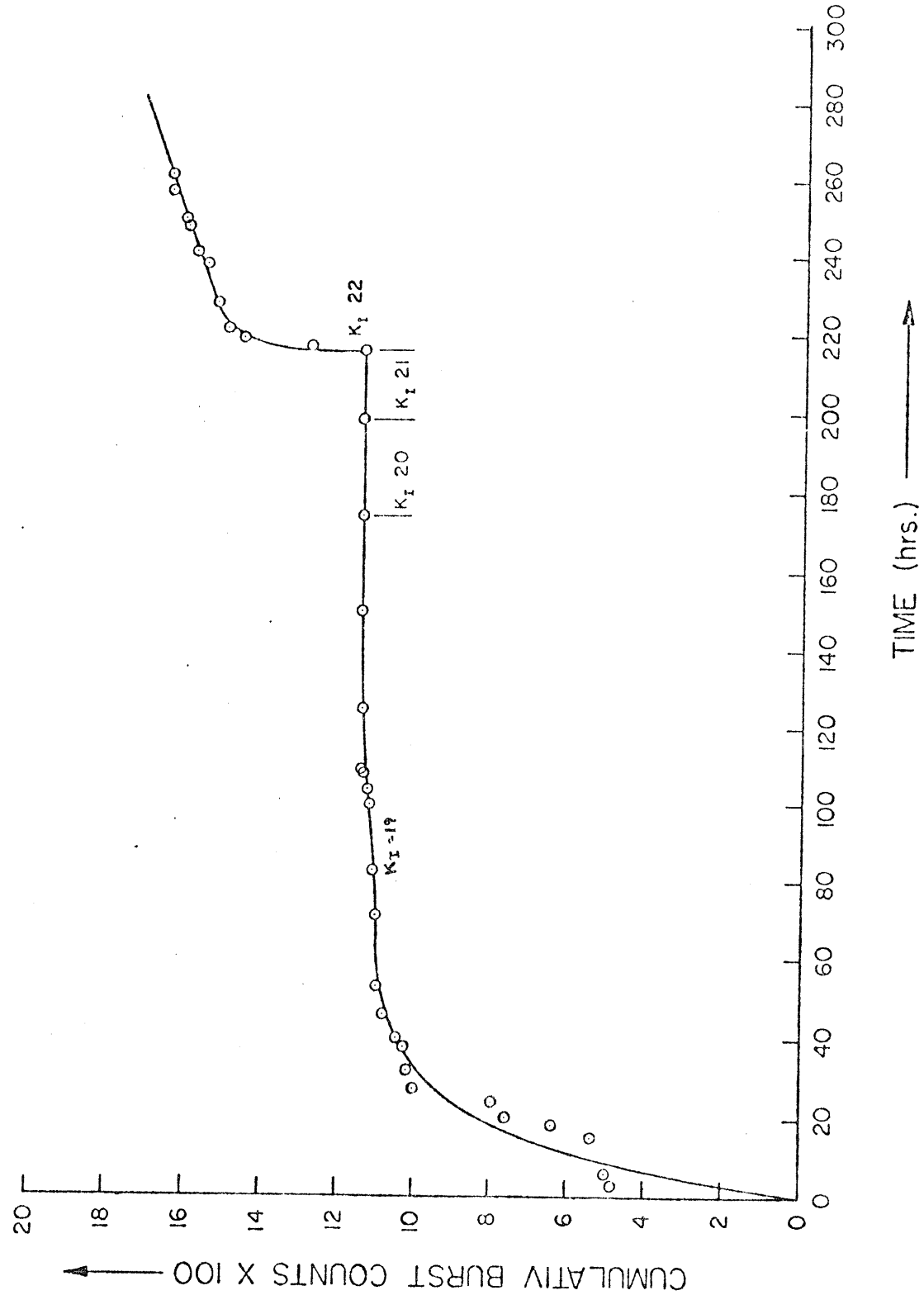

FIGURE 22. Effect of incremental K_I on slow crack growth in a stress-aged specimen at 100°C and K_I of 2.5 $MNm^{-3/2}$. Test Temperature 100°C.

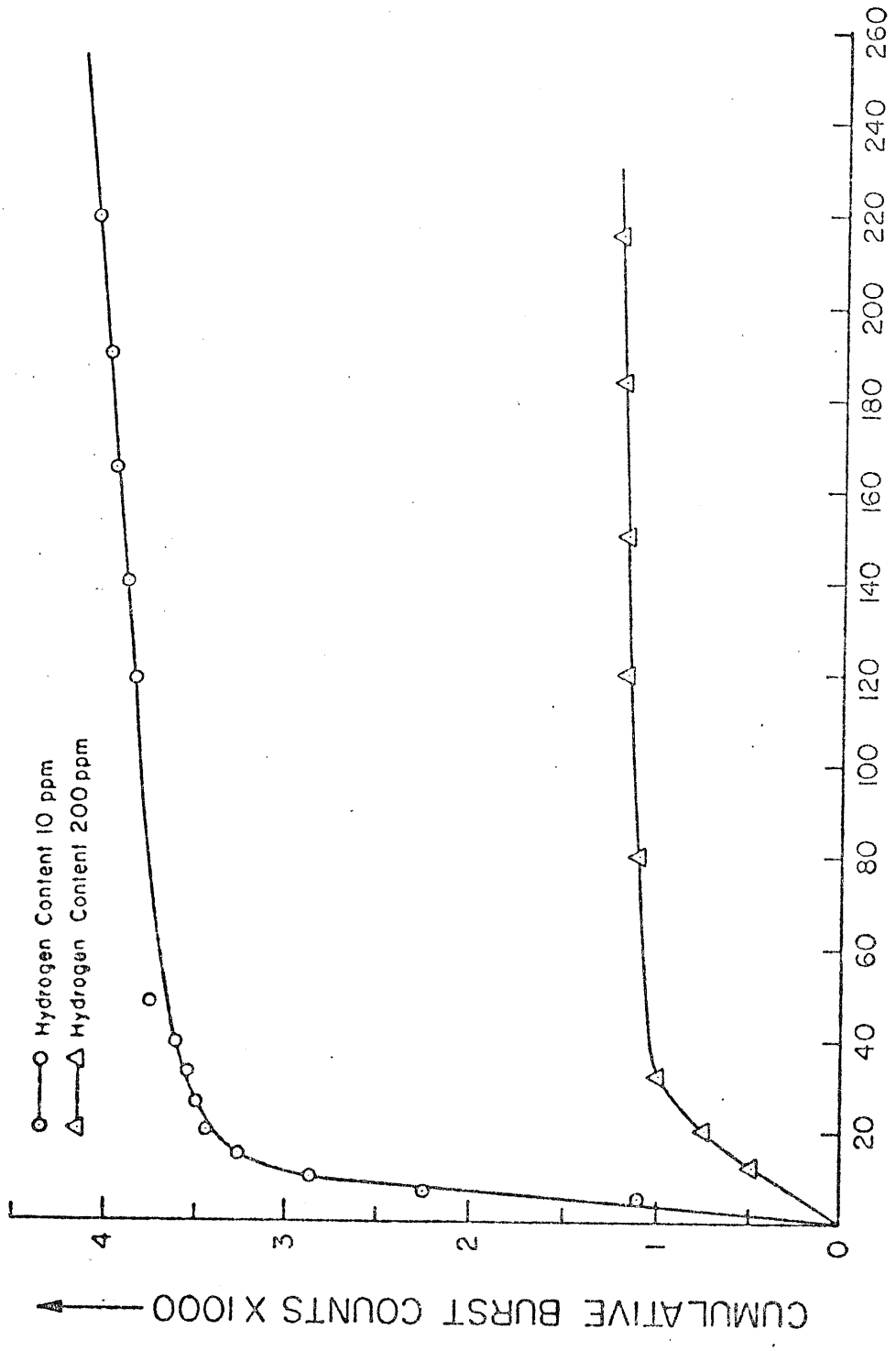

Fig. 23. Effect of Hydrogen Content on 'AE' Response of Slow Crack Growth in Stress Aged Specimens. Stress Aging at $K_I = 2.5\ MNm^{-3/2}$, Temp. = 100°C. Aging Time = 40 hrs.

each value. However, when K_I was further increased to 22 $MNm^{-3/2}$, AE activity reappeared with initial fast activity followed by a stable AE rate.

4.4 Fractography and Metallography

In conjunction with the above AE work, fractographic and metallographic studies on CT specimens were undertaken employing light and electron microscopy.

4.4.1 Hydride Particles

The hydride precipitates were observed in large numbers on the hydrided specimen surface (Plate 5). The precipitated particles lay parallel to the principle crack and were homogeneously distributed. In plate 5, a hydride particle can be seen just ahead of the crack tip, at D. The crack is widened at places, e.g. at A, B and C due to the presence (and cleavage) of hydride clumps along the crack. The particle length was of the order of 30-40 microns. A similar distribution and orientation of hydride particles was observed at the mid-section of the specimen. An enlarged view of the crack tip and hydride particles in an unhydrided specimen is presented in Plate 6. Region EF, FG and GH represent machined notch, fatique crack and slow crack-growth respectively. The hydride particles close to the crack tip are clearly seen at I.

4.4.2 Crack Growth

A typical fracture surface can be seen in Plate 7. The tarnished surface (B) before the fast fracture (C) represents

X 50

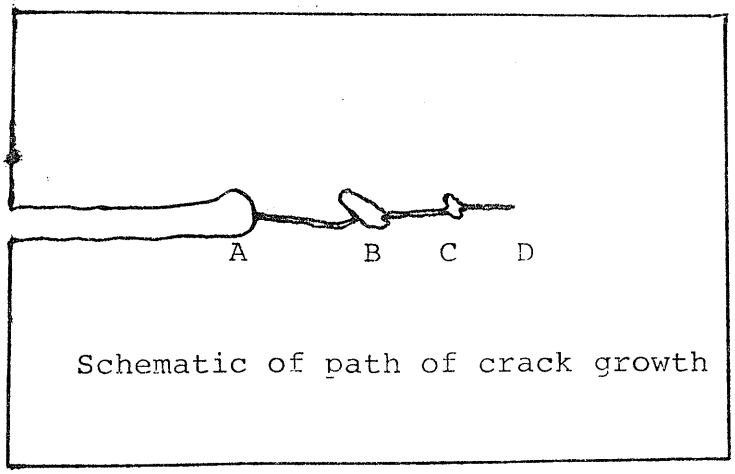

PLATE 5. Specimen Surface and the Distribution of Hydride Particles (Hydrided Specimen).

X 150

iew of Crack Tip and Adjacent Hydride Particles (Unhydrided Specimen)

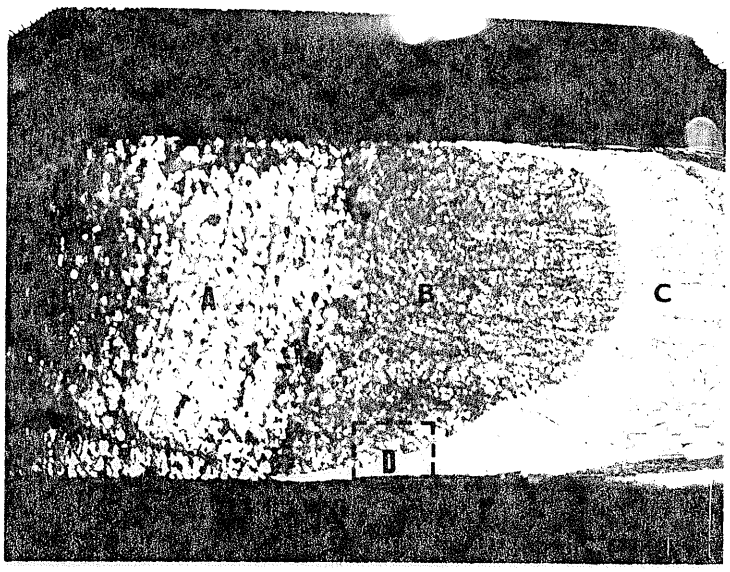

X 15

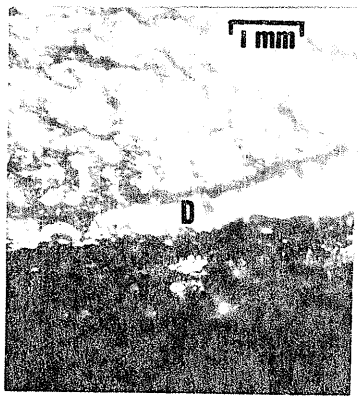

PLATE 7. Fracture Surface Showing Slow Crack Growth

slow crack growth. Region A belongs to fatique pre-crack. A shear lip zone (D) was observed close to the free surface of the specimen. The width of this zone depends on the stress intensity factor and is known to be roughly equal to the plastic zone size for the applied K_I. Crack tunneling at the centre is evident (Plate 7). In this specimen the crack length on the surface measured to 2.8 mm and at the centre 4.0 mm, indicative of increased crack growth at the centre. This observation indicates that the crack growth rate depends on the degree of crack-tip constraints. The growth was dominant at the centre where maximum 'transverse stress' due to plain strain condition existed, and on the surface, where plane stress condition was prevailant, little or no crack growth was observed.

4.4.3 Light Fractography

Plate 8 shows an optical micrograph of the fracture surface and a schematic of crack growth process. The direction of crack growth is from left to right. The region of fracture surface which is in focus indicates brittle fracture. The crack propagates on different planes (as seen in the schematic) and the fracture surface is formed by joining of these micro-cracks. Line of joining represents the striation indicative of discontinuous crack growth. Tear is prominant at A.

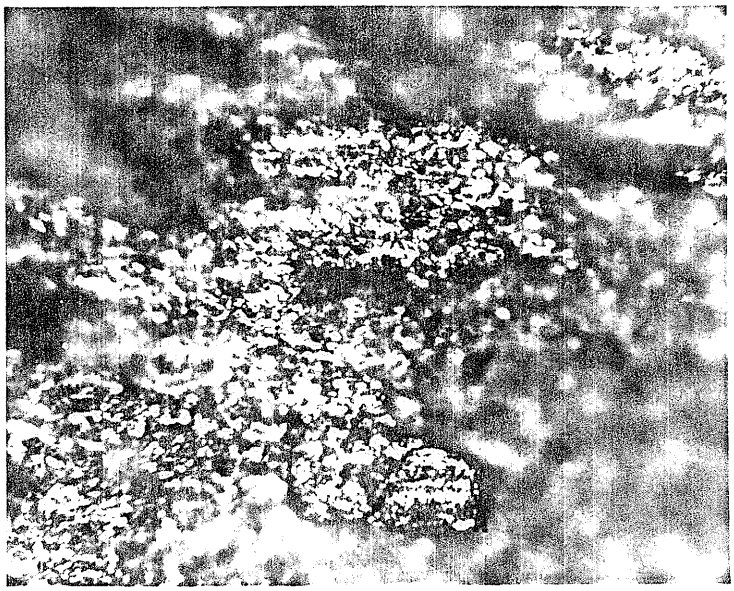

(a) x 570

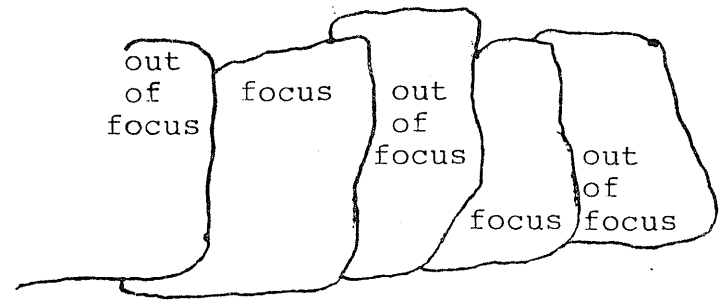

fracture surface
under optical
microscope

planes of fracture
surface observed above

PLATE 8. Optical Micrograph of Fracture Surface with schematic

4.4.4 SEM Fractography

The fracture surface consisted of dimples of various sizes and depth. A typical SEM fractograph can be seen in Plate 9a. The striations, containing the row of dimples, are visible at A and B, indicative of crack blunting and crack arrest. Another common feature was the presence of stringers as seen at C and D, and these supposedly contained a hydride particle before cracking. The stretch zones are also observed at the striations at E and F. The striation spacing is 35-40 microns with the stretch zones of 1.5-2 microns. The direction of crack growth is from bottom to top.

Plate 9b shows the fracture surface at a higher magnification. Some small dimples lie in bigger dimples. All the dimples have their tips pointing towards the direction of crack propagation. The surface in the foreground of dimples which carry hairline spikes such as at A, B, C and D is an indication of hydride cracking. Ductile striations at E and F indicate fast rate of growth due to high stress intensity.

Plate 9c is a fractograph of shear-lip region showing stringer on both sides of the ridge. The ridge appears because of the transition of stress state from plane strain to plane stress. The big dimples, on the right of the ridge, with stretched facets indicate fast fracture. The direction of crack growth was from bottom to top.

4.4.5 TEM Fractography

Large elongated dimples were observed on the replica of fracture surface indicating fracture under mode I. A typical

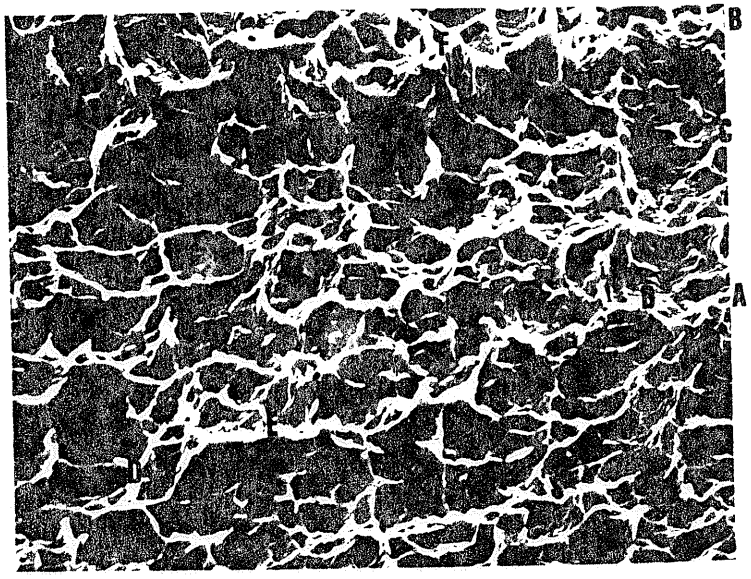

(a) x 1360

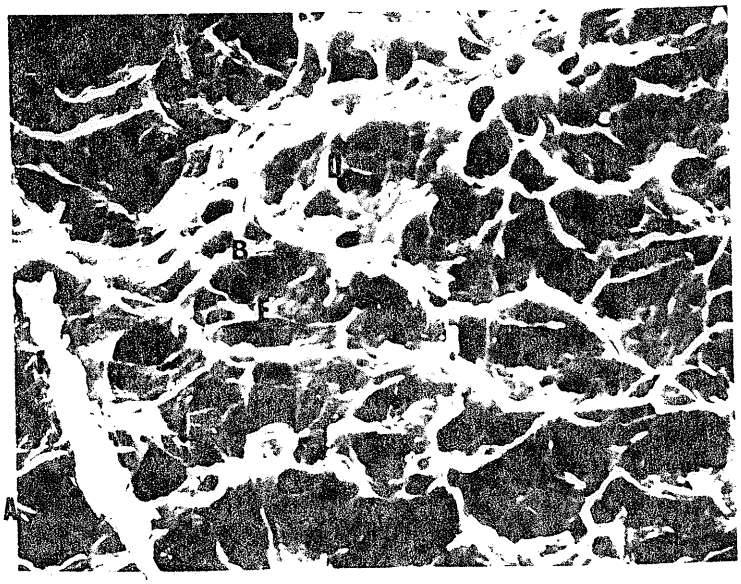

(b) x 2250

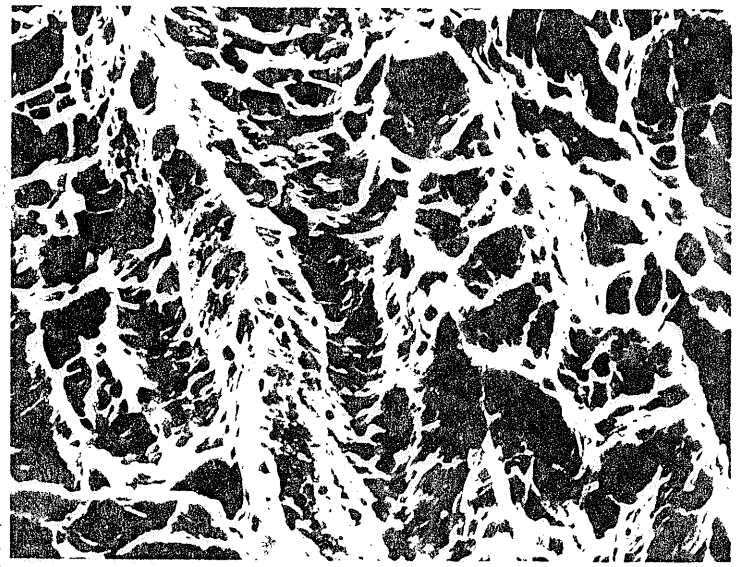

(c) x 1700

PLATE 9. SEM Fractographs of Fracture Surface

TEM fractograph can be seen in plate 10. The dimples are elongated in the direction of crack propagation. The dimples are indicative of void coalescence. The orientation of dimples is same all over the fracture surface. The striation marks at A, B and C are less evident due to poor quality replica. The ripple marks on the dimples strongly suggest that the crack growth takes place due to hydride embrittlement and the matrix is fairly ductile. The grain boundaries observed on the fractograph are from lucile grains.

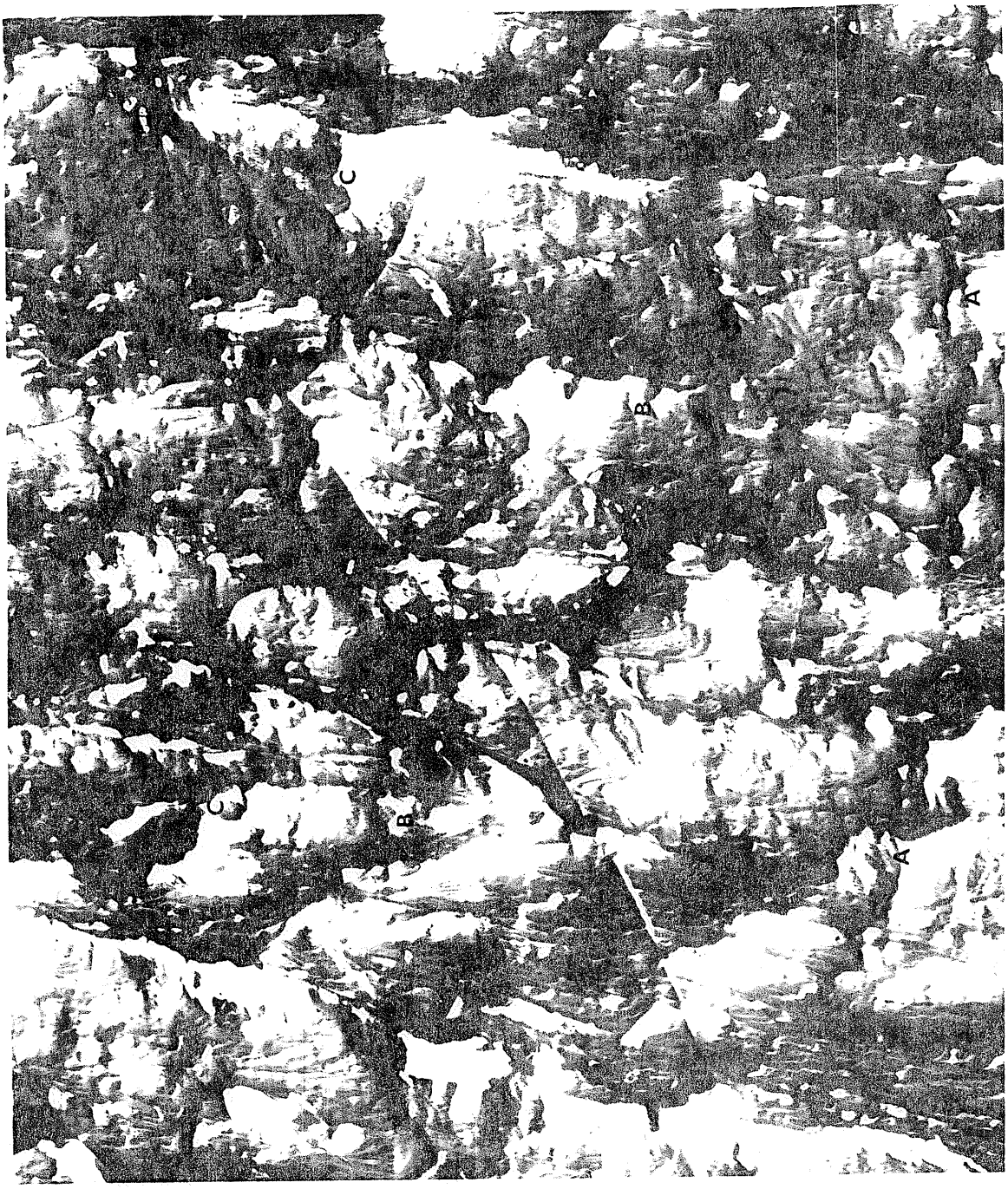

PLATE 10. TEM Fractograph X 4075

5. DISCUSSION

5.1 AE Signals and Fracture Mechanism

It has been conclusively documented in the studies concerning fracture mechanism in Zr-2.5% Nb system that the slow crack growth takes place through the brittle hydride particle precipitating ahead of the crack tip under high crack tip stress intensities. The crack is then arrested in Zr-matrix and further diffusion of hydrogen takes place towards the crack tip leading to further precipitation and crack growth. Thus the process of crack growth is discontinuous and is termed as hydrogen induced delayed cracking (HIDC). In AE monitoring, the observation of burst events strongly suggests that the fracture mechanism involves local embrittlement. The large bursts captured by waveform recorder suggest the same. ΣN-time plot (Fig.10) shows that the bursts are randomly spaced in time indicating that the crack growth process is discontinuous. The studies of temperature effects on AE show no cracking above high temperatures of 185-200°C which is the hydrogen solvus. This confirms the requirements of hydride particles for crack growth. All these AE findings support the aforesaid fracture mechanism, i.e. HIDC.

In addition, the fractography results show the presence of striations indicative of discontinuous crack growth under scanning and transmission electron microscopes. Features like hairline spikes in SEM (Plate 9b) and ripple marks in TEM fractographs suggest hydrogen embrittlement. Metallographic

studies revealed presence of hydride particles on the specimen surface and inside the specimen. Hence the fractography and metallography work is in support with AE results and the suggested models of slow crack growth in this alloy.

5.2 Signal Analysis

In view of AE results a model has been developed to physically explain the hydride precipitation and growth followed by cracking and is shown in a schematic (Fig.24). Stage I shows the plane of crack growth during fatique with initial distribution of pre-existing hydride particles. After loading, the particles from behind the crack front and away from the crack tip, dissolve and the hydrogen diffuses to the crack tip under the stress gradient (and under the influence of other factors explained in section 2.2.1). As explained in Dutton et al's model, the precipitation of hydrogen takes place and these precipitates grow by further diffusion and precipitation. It must be noted at this stage that all these precipitated particles, in the vicinity of crack tip, grow simultaneously from small sized particles to a minimum required length. The crack front is more or less flat before loading and the stress distribution is as shown in Fig. 24. As there is high stress distribution adjacent to the crack front, initially most of the particles precipitate and grow just ahead of the crack front resulting in hydride accumulation. This stage of accumulation of hydrides ahead of the crack tip is designated as stage II. No

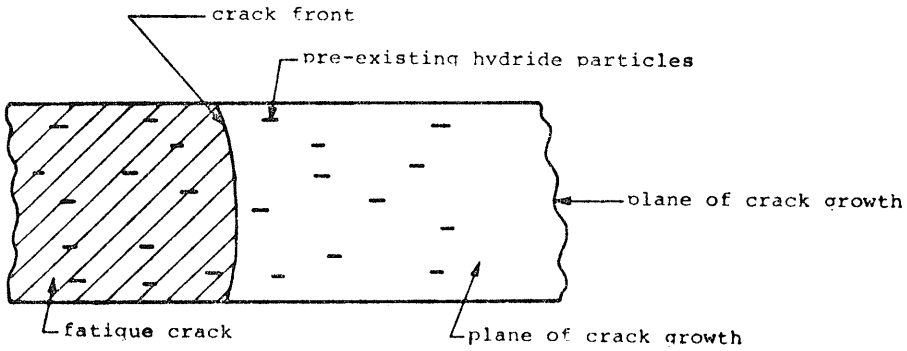

Stage I

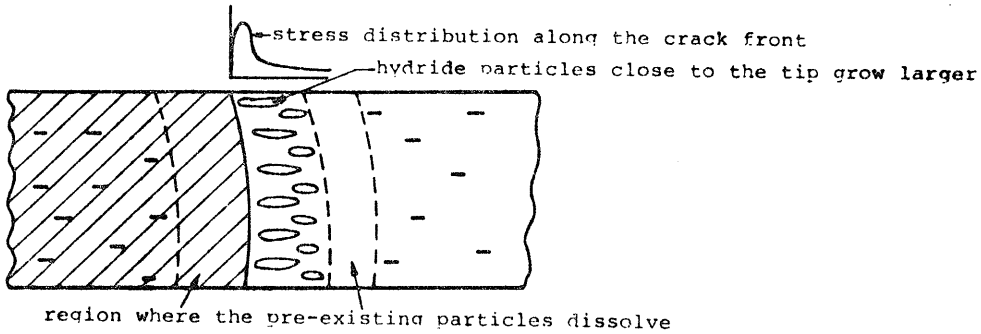

Stage II

(the particles at certain distance from the crack tip grow simultaneously and to the same size leading to hydride accumulation and multiple fracture)

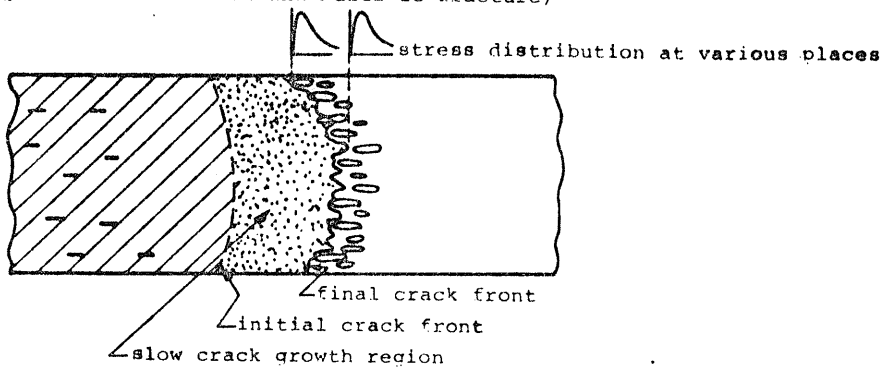

Stage III

(The particle size at a certain distance from initial crack front varies over the thickness)

Fig. 24 A Model of Hydride Precipitation and Cracking at all Stages

cracking event takes place during this accumulation for the reason that all the particles are growing evenly to the required length. As soon as the hydride particles grow to the critical length (which is sufficient to produce local embrittlement under high crack tip stresses), they crack. There could be more than one particle cracking simultaneously for the reason that more than one particle could grow to the same length, during the particle growth, if they initially lie at the same distance from the crack tip. As the particles crack, the stressfield moves with the advancement of the crack front (locally), and the process of diffusion, precipitation and particle growth is repeated accordingly in those local areas. It should be noted that all the growing particles initially may not lie at the same distance from crack front and so the particles lying at different distances from the crack front will grow to different lengths during the period of precipitation and particle growth when the first cracking takes place.

Now after the cracking starts, the crack front moves locally and so the stress field is random with respect to the initial crack front, and so is the process of precipitation and particle growth. Cracking of individual particles moves the crack front accordingly and the stress field is not uniform over the thickness of specimen any time after the cracking of the first few particles. Hence uneven crack front (observed experimentally) results in uneven growth of particles, i.e., the particles at a certain distance from initial crack

front will have different lengths. This is stage III where the accumulated particles have all cracked and a steady state is reached for the precipitation and growth of hydride particles. Once again it should be noted that in stage II, particles lying at a certain distance from the crack front will grow to the same length after a certain period due to a constant stress field; where as in stage III the particles precipitating at a certain distance from initial crack front will not grow to the same length after a fixed length of time. Since, even in stage III, the particles, at different distances from the initial crack front, grow simultaneously and at the same rate, under their local stress fields; they finally reach the required length at different times and crack individually leading to a constant rate of crack growth.

5.2.1 Incubation Period

As suggested by the above model, the incubation period is from stage I to stage II, i.e. the time required for the diffusion of hydrogen and its precipitation which ultimately initiates cracking. The crack incubation time is expected to depend on four factors: (i) test temperature, (ii) crack tip stress intensity, (iii) hydride orientation and distribution, and (iv) precipitation kinetics. The test temperature and stress intensity influence the precipitation kinetics whereas hydride orientation and distribution is, in principal, affected by the history of specimen and thermal treatments, prior to and during the test.

The crack tip stress intensity is affected by (i) crack radius, (ii) crack length, (iii) plane of the crack tip, and (iv) morphology of crack front. The crack tip radius and the plane of crack tip affect the incubation period very significantly and introduce irregularity in the characteristic incubation period that is expected in a given test. From the observations of several tests conducted, it can be said with reasonable certainty that the incubation period can be controlled by manipulation of temperature and stress intensity which affect the precipitation kinetics and particle growth. In a series of tests where precipitation and particle growth was assisted by low K_I value of 2.5 $MNm^{-3/2}$ prior to the crack growth test, little or no incubation period was observed. A similar argument has been extended by Coleman[52] but a reasonable correlation between observed incubation period and the particle growth rate could not be achieved.

In the experiments to study the effect of stress intensity on incubation period, it was observed that the increase in stress intensity decreases the incubation period. This is in accord with Colemans[52] results and confirms that high crack tip stress intensity results in higher stress gradient which accelerates hydrogen diffusion, hydride precipitation and particle growth, resulting in smaller incubation periods.

5.2.2 Fast Activity

The fast activity is the transition from stage II to stage III resulting from fast and multiple rupture of hydride particles that accumulate during incubation period. The accum-

ulation of hydrides occurs at stage II and the hydrides grow to certain length before rupture. As many of the particles reach this critical length growing simultaneously, they crack under high crack tip stress intensity giving rise to fast activity in AE monitoring. It is important to note here that fast activity is a characteristic behaviour of initial slow crack growth and is only a transient state between the start of cracking and the slow crack growth. It was observed that the absence of incubation period led to a reduction in fast activity. This is a reasonable observation because the absence of incubation period will result in lesser accumulation of hydrides. The results in Table 5 also indicate that the fast activity can be reduced by certain thermomechanical treatment. Typically for a 24-hour treatment the fast activity count rate was reduced by an order of magnitude on log-log scale (Fig.20). A similar state of fast activity has been also reported by Gerberich et al[53].

5.2.3 Stable AE

The crack growth at stage III of the suggested model results in stable AE. The cumulative burst count in this region was in linear relation with time (Fig. 11). The burst count rate was constant for extended periods suggesting that the crack in this region grows at a constant rate. Temperature did not have any significant effect on the burst count rate over the range of 100-140°C. Fig. 14 shows that the slope of two curves in region III is approximately the same.

This kind of behaviour can be explained by considering the effect of temperature on various parameters that control hydrogen diffusion and its precipitation. These parameters are diffusion coefficient and hydrogen solvus. The diffusion coefficient is increased with the increase in temperature, which facilitates hydrogen diffusion and its precipitation, but the hydrogen solvus is also increased by the increase in temperature which restricts the free hydrogen for precipitation. Thus over the temperature range of 100-140°C, the two parameters oppose the effects of each other and no significant change in AE rate is observed. When the temperature was raised above 140°C, a reduction in burst occurence was osbserved. Above 160°C the burst events drastically reduced and above 200°C no bursts were observed. The results suggest that no cracking or crack growth occurs above a limiting temperature since all the hydrogen is in solution. It has been established[40,41] conclusively that above hydrogen solvus, no cracking would occur. AE results supported this behaviour.

5.3 Burst Count and Crack Extension

The analysis of AE in terms of crack extension reveals that the burst signals emanate from cracking and can be related to the respective crack growth. This was an initial assumption which was examined by comparing the total number of burst count with the total area cracked during slow crack growth. Fig. 18 shows that the total burst counts are in direct proportionality with the area cracked. Similar conclusions

are reached by calculating the number of burst count per unit area. CT specimens, without stress aging treatment, were tested at different K_I values from 5 to 19 $MNm^{-3/2}$ and at temperatures of 100 or 140°C. Irrespective of variations in temperature the stress intensity, the ratio of burst counts to the cracked area is reasonably constant and suggests that for a certain material under any test conditions the cumulative burst counts will be directly proportional to the area cracked during the test, such that

$$\Sigma N \propto \Delta A \tag{5.1}$$

The relation is plausible for the reason that any material during cracking of a unit area will give out a certain amount of energy and this energy will increase proportionally for larger areas being cracked. The acoustic emission (burst signal in this case) consists of this energy in the form of stress waves which are detected on the surface of the material.

Equation (1) may be rewritten as

$$\Sigma N = D \cdot \Delta A \tag{5.2}$$

where D is the proportionality constant. The value of D ($.9 \times 10^4$ in our case, see Fig. 18) depends on two factors, (i) the monitoring system response that includes transducer characteristics, signal attenuation in the system, filter range, and system gain, and (ii) the material characteristics, e.g., microstructure, modulus of elasticity, tensile strength and fracture ductility. The time derivatives of equation (1) can be written as follows:

$$\frac{d(\Sigma N)}{dt} \propto \frac{d(\Delta A)}{dt} \tag{5.3}$$

or $\dot{N} \propto V$

or $\dot{N} = CV$ (5.4)

where $\dot{N}$ is the burst count rate or AE count rate, C the proportionality constant and V the crack velocity. Comparing the burst count rate $\dot{N}$ with the crack growth rate V in our tests, it was noted that the results followed equation (3) (Fig. 17). Similar expressons were established by Nadeau [32], and Evans and Linzer [30,31] for ceramic materials.

The establishment of such relationship is important in a way that the crack velocity could be estimated from the AE count rate at any time during the surveillance of pressure tubes and the flaw size could be calculated from the total burst counts. As an indirect approach the crack velocity can be measured in terms of counts/sec and the crack length in terms of total number of counts.

6. CONCLUSION

6.1 The following conclusions were drawn from the acoustic emission testing of CT specimens.

(a) Acoustic emission can successfully be used to monitor sub-critical cracking and crack growth in Zr-2.5% Nb. In addition, each cracking event can be detected and captured to observe on the oscilloscope screen as an exponentially decaying signal.

(b) The fracture mechanism could be identified by the use of acoustic emission technique. AE tests revealed that the mechanism operative during cracking and crack growth in Zr-2.5% Nb involves local embrittlement and that the crack growth process is discontinuous.

(c) There exists an incubation period for cracking to start. The crack incubation time decreases with increase in crack tip stress intensity and approaches infinity below a certain level which is the threshold stress intensity.

(d) After the initial loading the crack grows at a faster rate during the fast activity of AE. The increase in crack tip stress intensity significantly increases the fast activity rate. The conditions of temperature and stress influence the length of incubation period and affect the fast activity rate accordingly.

(e) A steady state is reached after approximately 50 hours of loading time. The stabilized AE is observed following

fast activity. The AE rate (burst count rate) in this region is the true measure of stable crack growth. The count rate remained constant for extended periods (up to 700 hrs).

(f) The frequency of burst event reduces as the temperature is increased above 140°C and abov e a certain level of temperature (185-200°C) the AE activity and so the cracking stops, to indicate the possibility of all the hydrogen in the solution. Such experiments could determine the hydrogen solvus in Zr-H system. It also confirms that the presence of hydride is a precondition for cracking to take place.

(g) Stress-aging treatment can reduce the AE rate, i.e. the crack growth rate considerably. A 60 hour treatment at 100°C and K_I of 2.5 $MNm^{-3/2}$ reduced the AE rate from 30 counts/hr to approximately 3 counts/hr in the stable AE region. This means the crack velocity was reduced to 10% of its original value by this treatment.

(h) The samples with higher hydrogen content (200 ppm) have higher crack growth rates compared to unhydrided specimens (10 ppm-H_2). Even the AE tests with initial stress-aging treatment of 40 hrs revealed different AE rates for the two samples.

(i) There exists a relationship between area cracked and the total burst counts. The total AE count and the AE count rate were directly proportional to the total cracked area and the crack velocity, respectively. This

was an important finding because the crack velocity could be measured in terms of AE count rate and the length of the crack can be estimated at any time during the surveillance of pressure tubes.

(j) The fractography results stand in support with AE observations but a quantitative correlation cannot be attempted for the test temperatures of 100-150°C. Higher temperatures are required for such attempts.

(k) The use of acoustic emission technique can be extended for prediction of ultimate failure because the quantitative measurements of flaw size and rate of failure can be estimated by AE monitoring of slow crack growth in Zr-2.5% Nb.

6.2 Future Work

Acoustic emission technique was used to study stage II of V-K curve, for the slow crack growth in Zr-2.5% Nb. AE monitoring may be employed to study stage I and the transition from stage I to stage II (of V-K curve). The incubation period and fast activity have been resolved to quite an extent under varied conditions of temperature and stress. Further investigations should be made by AE monitoring of slow crack growth after sharpening the fatique pre-crack to the threshold K_I to minimize the radius at the root of the crack. The technique can further be developed for dynamic subtraction of background noise by employing an anti-coincidence circuit which will trigger (for recording) only when a burst signal is received from the sample. The addition of a crack opening

displacement gauge is necessary for one to one correspondence of the burst signal with the crack growth. It will also provide information concerning fast activity.

Amplitude distribution analysis should be attempted for a quantitative analysis of burst height and the burst amplitude. It will also provide details of the statistical nature of the crack growth process. It can be identified by the amplitude distribution analysis if there is only one fracture mechanism operative during SCG at all temperatures or load conditions. The fracture behaviour of the two processes, namely, slow crack growth and fast fracture can be delineated and explained at a microscopic scale by amplitude distribution analysis.

REFERENCES

1. "Delayed hydrogen cracking of Zirconium alloy pressure tubes", AECL report 5691, Chalk River Nuclear Labs., Ont., Canada, October 1976.

2. Dunegan, H.L. and Tetelman, A.S., "Non-destructive characterization of hydrogen embrittlement cracking by acoustic emission techniques", Tech. Bull. DRC 106, Dunegan research corp., Livermore, Ca., 1971.

3. Ross,P.A., Dunn, J.T., Mitchel, A.B., Towgood, G.R., and Hunter, T.A., "Some engineering aspects of investigation into the cracking of pressure tubes in the Pickering reactors", AECL rept. 5261, CRNL, Chalk River, Ont., Canada, January 1976.

4. Liptai, R.B., Harris, D.O. and Tatro, C.A., "An introduction to acoustic emission", Amer. Soc. Test. Mats., STP 505, pp. 3-10.

5. Fisher, R.M. and Lally, J.S., "Microplasticity detected by an acoustical technique", Can. J. Phys., 45, 1967, pp. 1157-1162.

6. Schofield, B.H., "Acoustic emission under applied stress", Aeronautical Research Laboratories, U.S. Airforce, Wright-Patterson, AFD, Ohio, ARL-150, 1961.

7. Kerawalla, J.B., "An investigation of acoustic emission from commercial ferrous materials subjected to cyclic tensile loading", Ph.D. thesis, Univ. of Michigan, Ann Arbor, Michigan, 1965.

8. Mason, W.P., McSkimmin, S. and Shockley, W., "Ultrasonic observation of twinning in Tin", Physical Review, Vol.73, No.10, 1948, pp. 1213-1214.

9. Gillis, P.P., "Dislocation motion and acoustic emission", Amer. Soc. Test. Mats., STP 505, pp. 20-29.

10. Speich, G.R. and Fisher, P.M., "Acoustic emission during martensite formation", Amer. Soc. for Test. Mats., STP 505, pp. 140-151.

11. Liptai, R.G., Dunegan, H.L. and Tatro, C.A., "Acoustic emission generated during phase transformation in metals and alloys", Int. J. of NDT, IJNTA, Vol.1, 1969, pp. 213-221.

12. Woodward, B. and Harriss, R.W., "The use of signal analysis to identify sources of acoustic emission", Acoustica, Vol.37, No.3, 1977, pp. 190-197.

13. Gillis, P.P. and Hamstad, M.A., "Some fundamental aspects of theory of acoustic emission", Mat. Sci. Eng., Vol.14, 1973, pp. 103-108.

14. Tandon, K.N. and Tangri, K., "An acoustic emission study on deformation behaviour of strain aged Fe-3% Si samples", Mat. Sci. Eng., Vol.29, 1977, pp. 37-40.

15. Arrington, M., "Introduction to acoustic emission testing", Metrology and Inspection, October 1976.

16. Evans, A.G. and Liwzer, M., "Failure prediction in structural ceramics using acoustic emission", Journal of Amer. Cer. Soc., Vol.56, No.11, 1973, pp. 575-581.

17. Hamstad, M.A. and Chiao, T.T., "Structural integrity of fiber/epoxy vessels by acoustic emission, some experimental considerations", Lawrence Livermore Laboratories, Rept. UCRL 78198, Livermore, Ca., May 1976.

18. Webborn, T.J.C. and Rawling, R.D., "The monitoring of fatique crack in welded tubular joints", Proc. Inst. Acoust., London, U.K., December 1976.

19. Hartbower, C.E., Morais, C.F., Reuter, W.G. and Crimmins, P.P., "Acoustic emission from low cycle high stress intensity fatique", Eng. Fract. Mech., Vol.5, 1973, pp. 765-789.

20. Dunegan, H.L. and Harris, D.O., "Acoustic emission techniques", Experimental Techniques in Fracture Mechanics, ed. A.S. Kobayeshi, The Iowa State Univ. Press, Iowa, 1973, pp. 38-75.

21. Palmer, I.G. and Heald, P.T., "The application of acoustic emission measurements to fracture mechanics", Mat. Sci. Eng., Vol.II, 1973, pp. 181-184.

22. Dunegan, H.L., Harris, D.O. and Tatro, C.A., "Fracture analysis by use of acoustic emission", Eng. Fract. Mech., 1968, pp. 105-122.

23. Gerberich, W.W., Hartbower, C.E., and Crimmins, P.P., "Characterization of fatique crack growth by Acoustic Emission", Int. Jour. Fract. Mech., Vol.3, 1967, pp. 185-187.

24. Gerberich, W.W., Zackay, V.F., Parker, E.R. and Porter, D., Ultrafine Grain Metals, ed. J. Burke and V. Weiss,

Syracuse Univ. Press, Syracuse, 1970.

25. Dunegan, H.L. and Tetelman, A.S., "Non-destructive characterization of hydrogen embrittlement cracking by acoustic emission techniques", Eng. Fract. Mech., Vol.2, 1971, pp. 383-402.

26. Harris, D.O., Tetelman, A.S., and Darwish, F.A., "Detection of fiber cracking by acoustic emission", Amer. Soc. for Test. Mat., STP 505, pp. 238-249.

27. Palmer, I.G., Brindley, B.J. and Harrison, R.P., "The relationship between acoustic emission and crack opening displacement measurements", Mat. Sci. Eng., Vol.14, 1974, pp. 3-6.

28. Kirby, N. and Bentley, P.G., U.K.A.E.A., Rept. IX-802-72 1973.

29. Bentley, P.G., Burnup, T.E., Burton, E.J., Cowan, A. and Kirby, N., Proc. Inst. Mech. Engrs. Conf. on Periodic Inspection of Pressure Vessels, London, U.K., May 1972.

30. Evans, A.G. and Linzer, M., Failure prediction in structural ceramics using acoustic emission", Jour. Amer. Cer. Soc., Vol.56, 1973, pp. 575-581.

31. Evans, A.G., Linzer, M. and Russel, L.R., "Acoustic emission and crack propagation in polycrystalling alumina", Mat. Sci. Eng., Vol.15, 1974, pp. 253-261.

32. Nadeau, J.S., "Acoustic emission studies of slow crack growth", AECL report, PR-WCM-28, WNRE, Pinawa, 1975, pp. 186-194.

33. Gerberich, W.W. and Hartbower, C.E., "Monitoring crack

growth of hydrogen embrittlement and stress corrosion cracking by acoustic emission", Proc. Conf. fundamental Aspects of Stress Corrosion Cracking, Ohio State Univ., Columbus, Ohio, Nat. Assoc. Corro. Eng., Houston, Texas, 1971.

34. Cox, B., "A correlation between acoustic emission during stress corrosion cracking and fractography of cracking of Zircalloys", Corrosion, Vol.30, No.6, 1974, pp. 191-202.

35. Katz, Y. and Gerberich, W.W., "On the discontinuous nature of stress corrosion cracking in Titanium alloys", Jour. Fract. Mech., Vol.6, 1970, pp. 219-221.

36. Brihmadesam, J.S. and McCormic, N.J., "Acoustic emission analysis of stress corrosion cracking in type 304 stainless steels", Nuclear Technology, Vol.29, No.2, 1976, pp. 126-35.

37. Tatro, C.A., Liptai, R.G. and Moon, D.W., "Acoustic emission from formation and advancement of cracks", Presented at Intl. Conf. on Stress Corrosion Cracking and Hydrogen Embrittlement of Ironbase Alloys", Unieux-firming, France, June 1973.

38. Drouillard, T.F., Liptai, R.G. and Tatro, C.A., "Industrial use of acoustic emission for non-destructive testing", Amer. Soc. Test. Mat., STP 571, 1975, pp. 122-149.

39. Nuttal, K., "Some aspects of slow crack growth in hydrided Zr-2.5% Nb alloys", Proc. Symp. on Effect of hydrogen on behaviour of materials, Jackson Lake Lodge, Wyoming, Sept. 1975, pp. 441-451.

40. Coleman, C.E. and Ambler, J.F.R., "Susceptibility of Zirconium alloys to delayed hydrogen cracking", Presented at Symp. Amer. Soc. for Test. Mat., Quebec City, Que., Canada, August 1976.

41. Dutton, R., Woo, C.M., Nuttal, K., Simpson, L.A., and Puls, M.P., "The mechanism of hydrogen induced delayed cracking in Zr alloys", Presented at 2nd Int. Congress on hydrogen in metals, Paris, France, 6-11/vi/1977.

42. Dutton, R., Nuttal, K., Puls, M.P. and Simpson, L.A., "Mechanisms of hydrogen induced delayed cracking in hydride forming materials", Met.Trans.A.,Vol.8A,October 1977,pp.1553-62

43. Simpson, L.A. and Clarke, C.F., to be published in Met. Trans.

44. Simpson, L.A., private communication.

45. Simpson, L.A. and Nuttal, K., "On the factors controlling hydrogen assisted slow crack growth in Zr-2.5% Nb alloys", Presented at 3rd Int. Conf. on Zirconium in the nuclear industry, Quebec city, 1976.

46. Dulton, R. and Puls, M.P., "A theoretical model for hydrogen induced slow crack growth", Effect of hydrogen on behaviour of materials, ed. A.W. Thompson and I.M. Burnstein, Met. Soc., AIHE, New York, N.Y., 1976, pp. 516-528.

47. Takano, S. and Suzuki, T., "An electron optical study of Beta-hydride and hydrogen embrittlement of Vanadium", Acta met., Vol.22, 1974, pp. 265-274.

48. Simpson, C.J. and Ells, C.E., "Delayed hydrogen embrittlement in Zr-2.5% Nb alloys", J. Nucl. Mat. Vol.52, 1974, pp. 289-295.

49. Dutton, R. and Puls, M.P., "Comments on diffusion controlled stress rupture of polycrystalline materials", submitted to scripta Met.

50. ASTM standards for compact tension specimen for fracture toughness tests, ASTM-E-399-74, 1974.

51. Tangri, K., "Acoustic emission investigation of subcritical crack growth in Zr-2.5% Nb", Proceedings of the Institute of Acoustics, London, December 1976.

52. Coleman, C.E. and Ambler, J.F.R., "Acoustic emission during delayed hydride cracking in Zr-2.5% Nb alloy", Presented at the 2nd Inter. Congress on Hydrogen in Metals, Paris, France, June 1977.

53. Gerberich, W.W., Hartbower, C.E. and Crimmins, P.P., "Spontaneous strain aging as a mechanism of slow crack growth", J. Weld., Vol.47, 1968, pp. 4433-4435.

APPENDIX A

A.1 Transducer Characteristics and Response

The response of transducer D9205M2 under varied test conditions are given below:

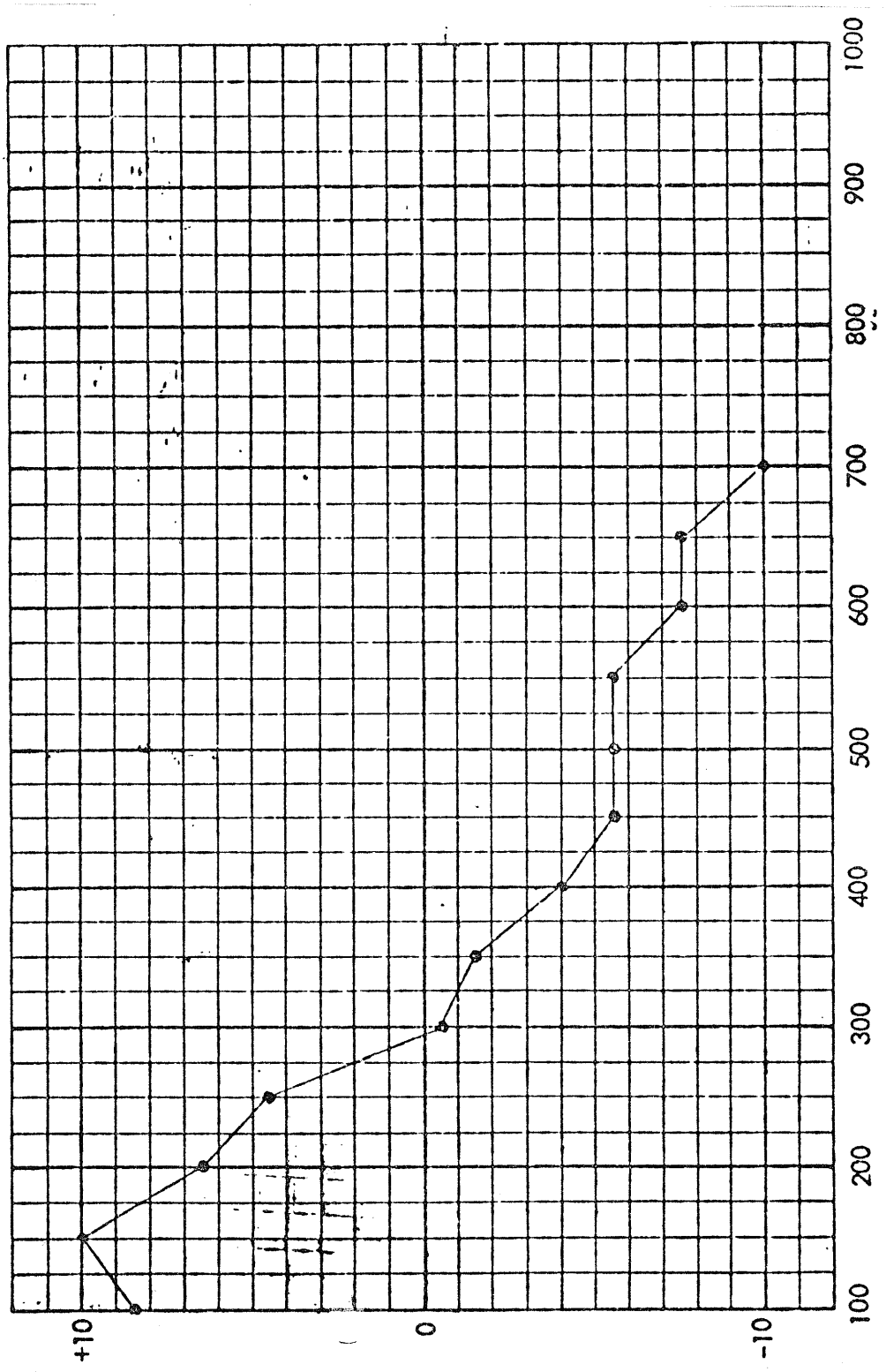

Fig. 1/A.1 Relative Responses of the Transducer

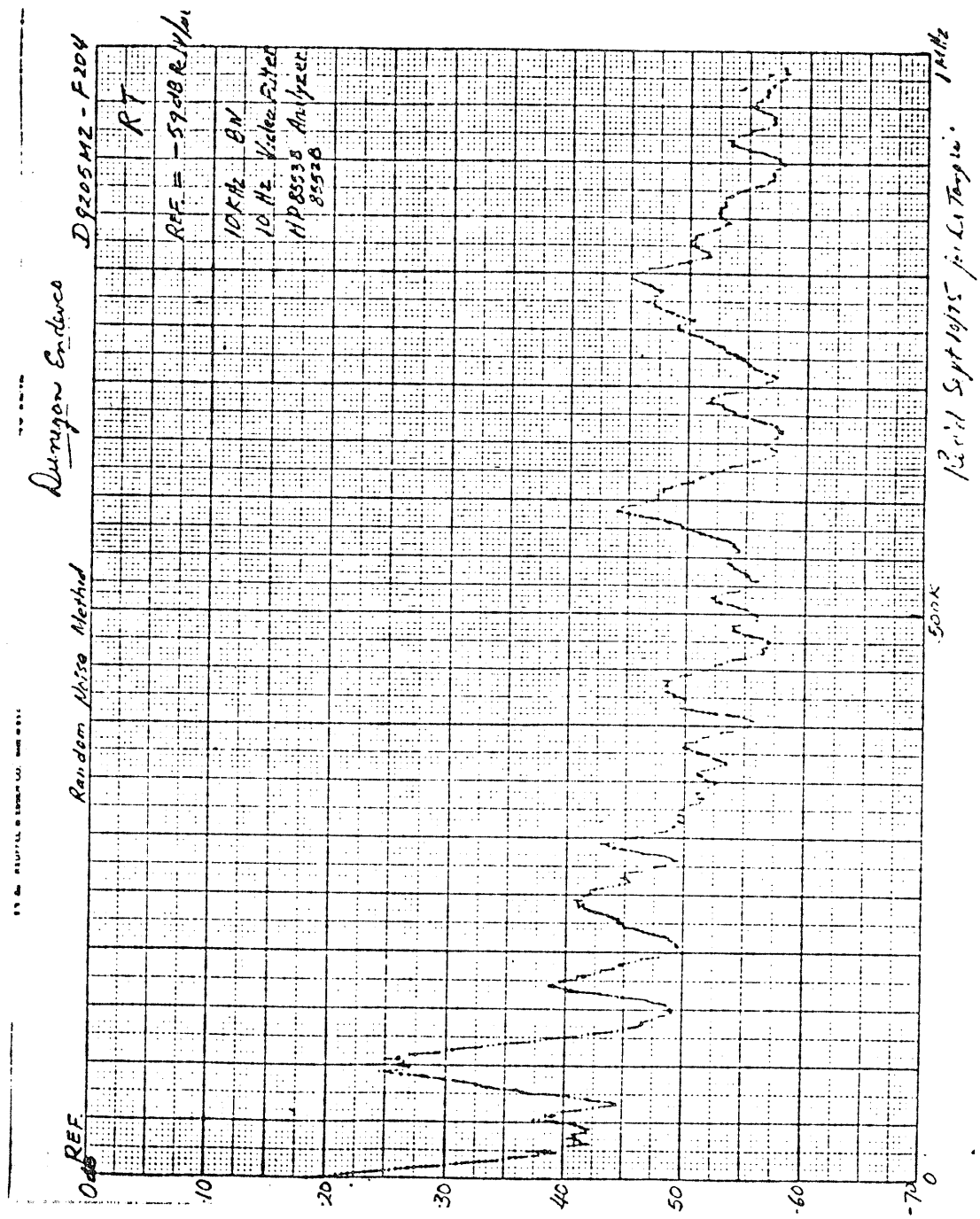

Fig. 2/A.1 Characteristic Response of the Transducer at Room Temperature

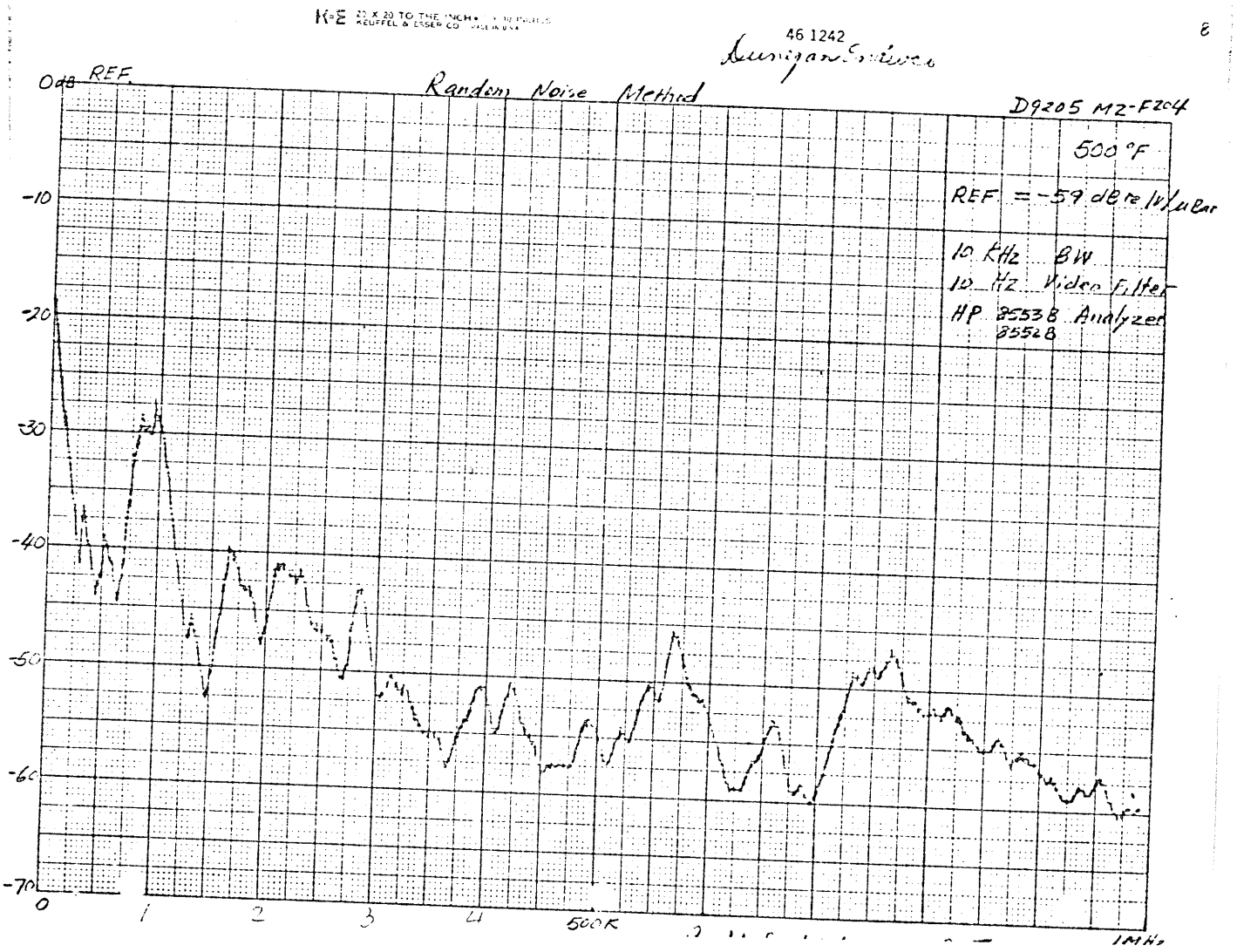

Fig. 3/A.1 Characteristic Response of the Transducer at 500°F

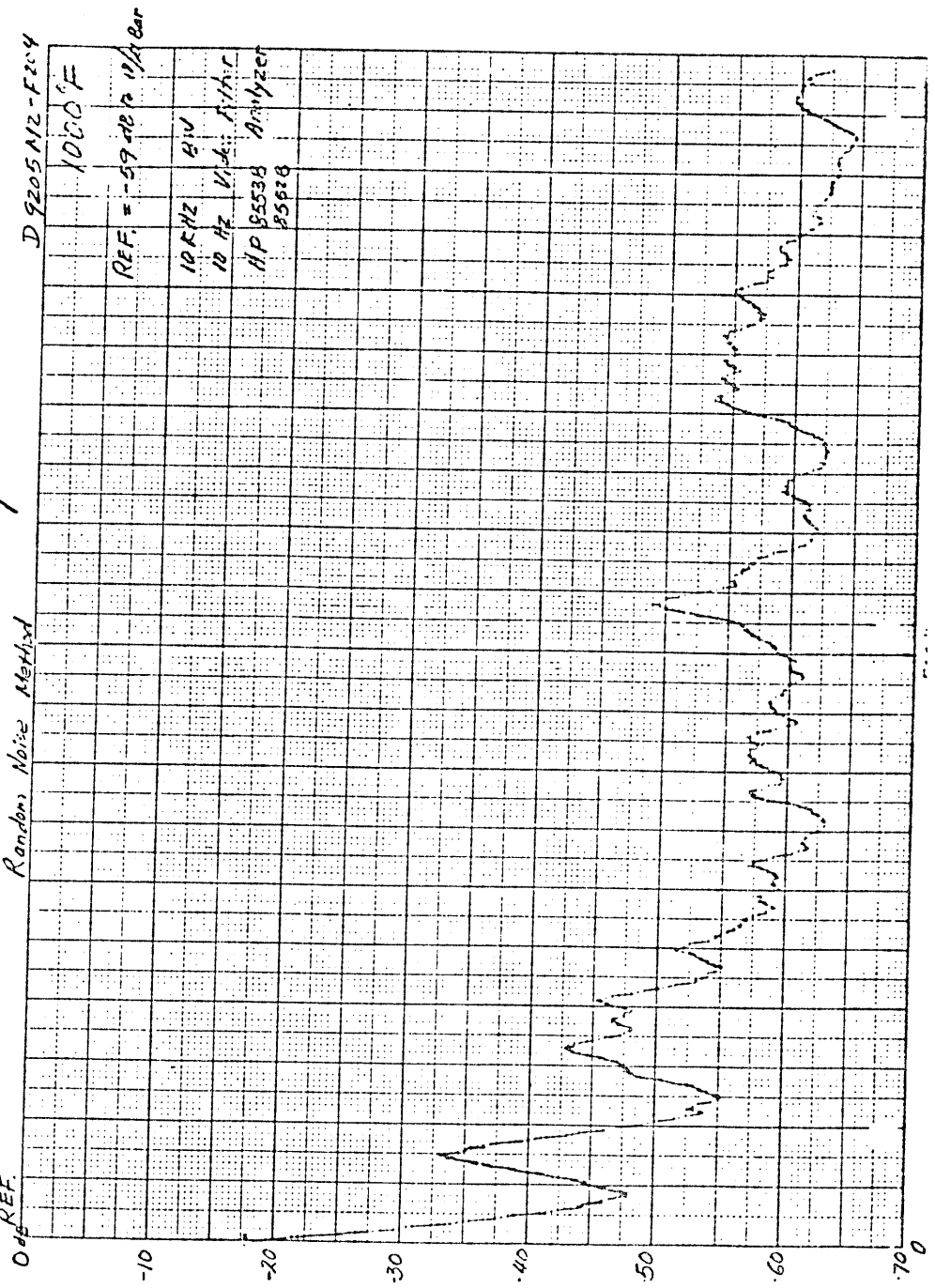

Fig. 4/A.1 Characteristic Response of the Transducer at 1000°F

APPENDIX B

B.1 System Calibration with Signal Processor 920

In few experiments signal processor, Model 920 Dunegan Research Corp., with a built in threshold comparator level was used. It monitored AE signals by ring counting mechanism over a prefixed threshold voltage of 1 volt, or a floating threshold voltage for dynamic subtraction of the background noise. The system had facility to record amplitude distribution of AE signals in normal linear, linear sum, normal sum or log sum forms. The signal processor was connected to the system as shown in Fig. (at the place of counter). The Brookdeal amplifier was substituted by 801P differential preamplifier (Dunegan research corp.) with a fixed gain of 40 db.

Figure 24 showing signal log amp characteristic and Table 6 for gain-amplitude trigger level, were used for calibration of the system. After the set-up was made, the gain to count a signal was estimated. The trigger level across 95 db gain reads 17.8 μv of trigger level (Table 6). After the preamplification of 40 db by 801 P preamplifier, the required trigger level estimated to 1.78 μv which corresponds to 26 db on scale onto the right of Figure 24. Thus a threshold level of 26 db was used to cut off the background noise and monitor the signal. A gain of 55 db was provided on the counter unit for the total of a 95 db gain to count the signals. The AE was monitored successfully with this unit.

Table 6. Gain-Amplification-Trigger Level* (Dunegan)

Db re 1v/xb Gain	Amplification	Trigger Level (μ.v.)	Db Gain	Amplification	Trigger Level (μ.v.)
20	10	100,000	89	28180	35.5
40	100	10,000	90	31620	31.6
60	1000	1,000	91	35480	28.2
61	1121	892	92	39810	25.1
62	1259	794	93	44670	22.4
63	1412	708	94	50120	20.0
64	1584	631	95	56230	17.8
65	1779	562	96	63100	15.8
66	1995	501	97	70790	14.1
67	2239	447	98	79430	12.6
68	2512	398	99	89130	11.2
69	2818	355	100	100,000	10.0
70	3162	316			
71	3548	282			
72	3981	251			
73	4467	224			
74	5012	200			
75	5623	178			
76	6310	158			
77	7079	141			
78	7943	126			
79	8913	112			
80	10000	100			
81	11210	89.2			
82	12590	79.4			
83	14120	70.8			
84	15840	63.1			
85	17790	56.2			
86	19950	50.1			
87	22390	44.7			
88	25120	39.8			

Table: Trigger levels at various Db gain re 1 v/μb and 1V. Trigger Level after amp.

* Trigger level-lowest voltage amplified to 1 volt at said gain level.

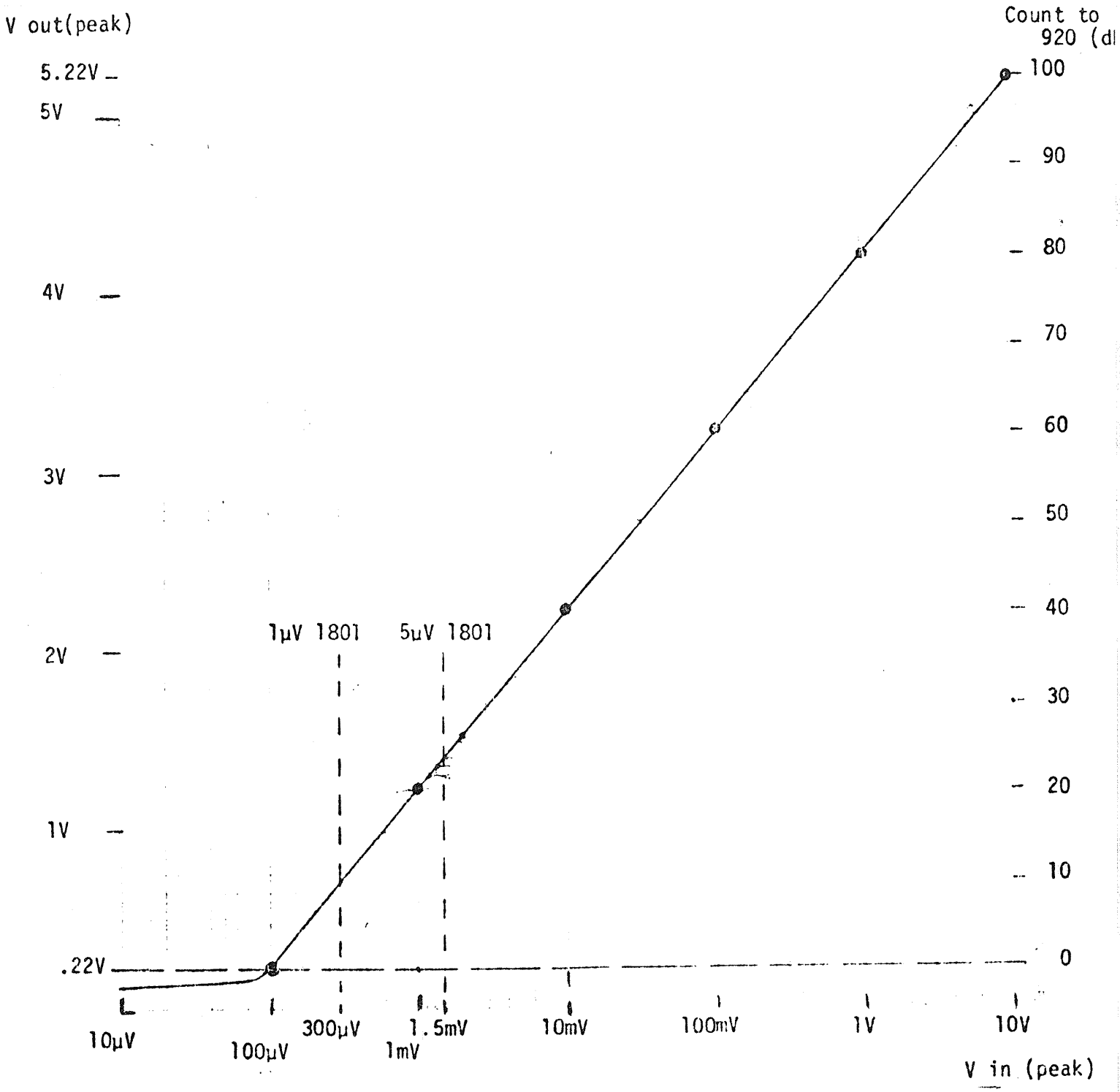

FIGURE 1/A.2 Log-Amp Characteristic of System With Model 920

APPENDIX C

Acoustic Emission Termonology

Acoustic Emission

Acoustic emission is a transient elastic wave generated by the rapid release of energy within a material.

Acoustic Event

An acoustic event is the rapid physical change in the material, that releases energy appearing as acoustic emission.

Acoustic Signal

An acoustic signal is an observed signal obtained by detection of acoustic emission.

Background Noise

Background noise is an erroneous signal coming from the ambient, electronic leakage or malfunctioning of the system

Burst Signal

Burst signal is an exponentially decaying signal (with time) captured on the oscilloscope screen, appearing as a jump in the continuous monitoring of acoustic emission.

Continuous Signal

A continuous signal is an apparently sustained signal from rapidly occuring acoustic emission events.

Noise Transient

Noise transient is a transient signal occuring over less

than 0.01 μ sec. It is usually from line or building noise, called as line or building transient.

Threshold Level

Threshold level is a comparator level (usually 1 volt) with which an acoustic signal is compared.

Acoustic Emission Count

Acoustic emission count is a weighted measure of acoustic events which have occurred over a given time period.

Burst Count/Burst Height

Burst count or burst height is the number as many times a burst signal crosses the threshold level on the +ve cycle. Such a counting method is known as ring-down counting mechanism.

Burst Count Rate/AE Count Rate

Burst/AE Count rate is a weighted measure of Burst/AE counts over unit period of time.

Frequency of AE Burst

It is the occurrence of burst signals over a given period of time. Ambiguity of the term suggests its use be limited.

Incubation Period

Incubation period is the time to incubate cracking and crack growth. Experimentally, it is the time taken for the first burst event to occur from the start of the test.

Interburst Period

Interburst period is the time lapse between any two consecutive burst events.

Fast Activity

It is the rapid occurrence of burst events for the initial period of AE monitoring.

Stable AE

It is the stabilized rate of occurrence of AE/bursts following the fast activity.